

submitted to the AJ, May 5, 2006; accepted, Aug. 30, 2006

Circumstellar atomic hydrogen in evolved stars¹

E. Gérard

*GEPI, UMR 8111, Observatoire de Paris, 5 place J. Janssen, F-92195 Meudon Cedex,
France*

Eric.Gerard@obspm.fr

and

T. Le Bertre

*LERMA, UMR 8112, Observatoire de Paris, 61 av. de l'Observatoire, F-75014 Paris,
France*

Thibaut.LeBertre@obspm.fr

ABSTRACT

We present new results of a spectroscopic survey of circumstellar H I in the direction of evolved stars made with the Nançay Radiotelescope. The H I line at 21 cm has been detected in the circumstellar shells of a variety of evolved stars: AGB stars, oxygen-rich and carbon-rich, Semi-Regular and Miras, and Planetary Nebulae. The emissions are generally spatially resolved, i.e. larger than $4'$, indicating shell sizes of the order of 1 pc which opens the possibility to trace the history of mass loss over the past $\sim 10^4 - 10^5$ years. The line-profiles are sometimes composite. The individual components have generally a quasi-Gaussian shape; in particular they seldom show the double-horn profile that would be expected from the spatially resolved optically thin emission of a uniformly expanding shell. This probably implies that the expansion velocity decreases outwards in the external shells (0.1–1 pc) of these evolved stars.

The H I line-profiles do not necessarily match those of the CO rotational lines. Furthermore, the centroid velocities do not always agree with those measured in the CO lines and/or the stellar radial velocities. The H I emissions may also be shifted in position with respect to the central stars. Without excluding the possibility of asymmetric mass ejection, we suggest that these two effects could also be related to a non-isotropic interaction with the local interstellar medium.

H I was detected in emission towards several sources (ρ Per, α Her, δ^2 Lyr, U CMi) that otherwise have not been detected in any radio lines. Conversely it was not detected in the two oxygen-rich stars with substantial mass-loss rate, NML Tau and WX Psc, possibly because these sources are young with hydrogen in molecular form, and/or because the temperature of the circumstellar H I gas is very low (< 5 K).

Subject headings: stars: AGB and post-AGB – (stars:) circumstellar matter – stars: late-type – stars: mass-loss – (ISM:) planetary nebulae: general – radio lines: stars

1. INTRODUCTION

Hydrogen is the most abundant element in the atmospheres of Asymptotic Giant Branch (AGB) stars and in their outflows. It may be found in the form of atomic hydrogen, H I, or molecular hydrogen, H₂, besides relatively minor (in abundance) species. The fraction of hydrogen in each of these two forms is an important factor controlling the atmospheric structures of red giants and also the winds which develop from their atmospheres (e.g. Lamers & Cassinelli 1999).

It is therefore of interest to study the circumstellar environments of AGB stars in the low excitation hydrogen lines. Unfortunately molecular hydrogen is presently difficult to detect because its lowest rotational lines lie in a region of the spectrum which cannot be accessed from the ground, and because a high spectral resolution is needed.

On the other hand atomic hydrogen has a line at 21 cm in an easily accessible, and well protected, region of the radio spectrum. However the observations are difficult because the intensity is weak and above all because there is a contamination by interstellar hydrogen along the same lines of sight. For a long time these difficulties have limited the H I observations of AGB sources to *o* Cet (Bowers & Knapp 1988, BK1988). Nevertheless we recently readdressed this question with the upgraded Nançay Radiotelescope and could detect this line in emission towards several AGB sources. We have already presented our results on four of them: RS Cnc (Gérard & Le Bertre 2003, Paper I), EP Aqr and Y CVn (Le Bertre & Gérard 2004, Paper II) and X Her (Gardan et al. 2006, Paper III). We detected these four AGB sources with a good signal-to-noise ratio and showed that the line

¹This paper is dedicated to the memory of Marie-Odile Mennessier (1943-2004).

profiles are composite. The individual components have Gaussian-like profiles, although in some cases a rectangular profile could be fitted as well. The H I emissions are spread over a velocity range confined to the total CO velocity extent. However, we noted that sometimes the central velocities in CO and H I do not coincide exactly. Furthermore, in Paper I, we argued that atomic hydrogen is present already in the stellar atmosphere of the central star (RS Cnc) which might even be devoid of molecular hydrogen. In Paper II we could resolve angularly two circumstellar shells, and show that H I may be present at large distances from the central stars, 0.5 pc or more for EP Aqr. The H I data display a large scale asymmetry suggesting that asymmetric structures may show up early in the AGB phase (EP Aqr & X Her), well before the planetary nebula phase. In the case of the source associated to Y CVn, the H I data even seem to probe a large region extending out to where the stellar outflow is interacting with the Interstellar Medium (ISM).

It thus appears that the H I emission line profiles, when observed with a good signal-to-noise ratio and a fair removal of the ISM contamination, may reveal important clues on the physics of stellar outflows and their kinematics. Also, as atomic hydrogen has a long lifetime in the ISM, it can be used to trace circumstellar envelopes out to large radial distances. In the present paper, we give results on 22 new sources for which we have now good quality spectra, or good upper limits. The main emphasis of our programme is put on AGB sources and we have tried to select a variety of representative specimens in terms of variability types, chemical composition, mass loss rates, etc. In addition, we have also included two planetary nebulae in order to sample more completely the post-main-sequence evolution of stars of low and intermediate masses. Two of our sources have already been observed in H I with the Very Large Array (VLA), *o* Ceti (BK1988) and NGC 7293 (Rodríguez et al. 2002, R2002). This allows a useful comparison between single-dish and interferometric data.

2. OBSERVATIONS

2.1. Observing Procedure

The observations have been performed with the Nançay Radiotelescope (NRT). The NRT is a meridian instrument with a rectangular effective aperture of $160\text{ m} \times 30\text{ m}$. The HPBW at 21 cm is $4'$ in the East-West direction and $22'$ in the North-South direction. It has been upgraded (van Driel et al. 1996) and reopened to observations in 2001. The point source efficiency is 1.4 K Jy^{-1} at 21 cm and the total system noise $\sim 35\text{ K}$. The autocorrelator has 8192 channels split in 4 banks of 2048, recording the linear ($\text{PA} = 0$ and 90°) and circular polarisations. For our programme we consider only the total intensity (Stokes parameter I).

Two modes of observation have been used. In the frequency-switch (f-switch) mode, the data are acquired on source with a spectral resolution of 0.08 km s^{-1} and a bandwidth of 160 km s^{-1} . This mode is very useful to check the level of interstellar H I emission in the direction of the source. A first indication of this level can be obtained by consulting the existing galactic H I surveys (e.g. Hartmann & Burton 1997), but their sensitivity limits are too high to readily select directions in which it might be possible to detect circumstellar H I with a priori minimum background confusion. In the course of our programme, we characterize qualitatively the confusion by “weak”, “mean” and “high”. These indications are reported in Table 2 (col. 2, see Sect. 2.2). They are based on Hartmann & Burton’s results that are obtained with a single dish of HPBW $\sim 0.5^\circ$, as well as on our own f-switch observations. It should be noted that the impact of confusion depends on the telescope beam size and on the observing strategy, in particular single-dish versus interferometric mode. Exceptionnally H I from the source can be seen directly on the f-switch spectra (e.g. Y CVn, Paper II).

For the circumstellar H I observations proper we use the position-switch mode, in which the telescope field of view (f.o.v.) is alternated between the on-source position and 2 off-source positions, placed symmetrically in the East-West direction. We refer to Paper II for a more detailed description of our observing procedure. It has proven to be most effective in separating the circumstellar emission from the interstellar one. A reason for this success comes from the fan beam shape ($4' \times 22'$) of the telescope that allows a good East-West discrimination of the circumstellar envelope against the galactic H I background. It should be noted that this procedure works perfectly when the intensity of the background varies linearly in right ascension across the region centered on the source. However, if the background presents a quadratic variation, or variations of higher *even* orders, spurious spectral features may appear. Such features generally grow rapidly with increasing separation between the 2 off-positions, which allows to identify them.

In general we selected a bandwidth of 80 km s^{-1} with a spectral resolution of 0.04 km s^{-1} . For some sources where a large expansion velocity is expected from CO line data or where galactic confusion affected part of the spectrum, we have used a bandwidth of 160 km s^{-1} . The data are then smoothed to give a final spectral resolution of 0.32 km s^{-1} . Except when mentioned otherwise, this resolution is used by default in the figures (Sect. 2.2).

Finally, the source sizes are often comparable or larger than the NRT beam ($4'$ in the East-West direction). The intensity increases with beam throw and then reaches a maximum for $\pm n$ beams when both off-positions (East and West) lie entirely outside the source. We then reconstruct the total intensity (s_{tot}) by summing up the source fluxes in the different off-positions (s_k) and in the central position (s_0):

$$s_{tot} = \sum_{k=-n+1}^{n-1} s_k \quad (1)$$

This is done by combining the position-switch spectra obtained at $\pm k$ beams ($C_k EW$) in the following expression:

$$s_{tot} = (2n - 1) \times C_n EW - 2 \sum_{k=1}^{n-1} C_k EW \quad (2)$$

n being such that the intensity in 2 successive position-switch spectra is the same, i.e. $C_{n+1} EW = C_n EW$. The radius of the source can then be estimated to $(n - 1) \times 4' \pm 2'$. Equ. (2) assumes that the background varies linearly across the sky. On the other hand it makes no assumption on the brightness distribution of the source. For an unresolved source ($\phi \leq 4'$), Equ. (2) reduces to:

$$s_{tot} = C_1 EW = C_2 EW = C_3 EW, etc. \quad (3)$$

In the figures (next Section), the position-switch spectra ($C_1 EW$, $C_2 EW$, etc.) are shown in the upper panels, and their averages and the final spectra (s_{tot}) are displayed at the bottom (continuous and dashed curves, respectively).

The average spectrum has a physical meaning only for an unresolved source (Equ. 3). However, the resulting signal-to-noise ratio is in general higher than for the total spectrum, so that spectral details are sometimes better seen on the average profile (see, e.g. below, Y UMa or R Peg). The difference between the two sets of spectra is the result of the source resolution by the $4'$ beam.

2.2. Sample of Sources

Table 1 lists the sources discussed in the present paper. We give the common name used in this work (col. 1), the IRAS identifier (col. 2), and some basic data. Except if mentioned otherwise, the spectral type (col. 3), the variability type (col. 4) and the period (col. 5) are taken from SIMBAD, directly or through the VizieR Service. The distances (col. 6) are in general deduced from the Hipparcos parallaxes. Next (col. 7), we give an estimate of the stellar effective temperature, T_{eff} . This datum is important because hydrogen in the stellar atmosphere and in the inner circumstellar envelope is expected to be mostly atomic

for $T_{\text{eff}} > 2500$ K and molecular for $T_{\text{eff}} < 2500$ K (Glassgold & Huggins 1993, GH1983). Finally we give the LSR radial velocity (V_{lsr} , col. 8), the expansion velocity (V_{exp} , col. 9), and the mass loss rate, estimated in general from CO rotational line data. These data are useful because both the central velocity and the velocity extent of the HI lines are expected to be close to those given by the CO lines. In general CO data from different observers are consistent within ± 2 km s $^{-1}$. When no CO data are available (δ^2 Lyr, ρ Per, α^1 Her, U CMi, NGC 6369), we adopt equivalent parameters from optical observations. Unfortunately, optical data seem less reliable than CO data (± 5 km s $^{-1}$), perhaps in part due to the stellar variability. Except for U CMi, circumstellar envelopes have been detected around all sources of our sample, either in the CO radio lines, or in optical lines.

In Table 2, we give the parameters characterizing the HI emissions. In general these emissions can be fairly well fitted with a Gaussian. We derive the LSR central velocity, V_{cent} (col. 4), a full width at half maximum, FWHM (col. 5), and a peak intensity, F_{peak} (col. 6), obtained from an unconstrained positive Gaussian fit to the integrated flux (s_{tot} ; Equ. 2). In the cases of composite profile (Y UMa, R Peg), two such Gaussians are also fitted to the average profile in the lower panel of the corresponding figure. When part of the spectrum is affected by interstellar confusion it has been excluded from the range used for the Gaussian fit. In such cases, the part of the spectrum which is affected is always that closest to 0 km s $^{-1}$ LSR. The Flux (col. 7) is estimated from the integral of the s_{tot} Gaussian fit and therefore only takes into account the extension of the source in right ascension. Finally the hydrogen mass, M_{HI} (col. 8), is derived from the Flux and for the distance, d (Table 1). We assume negligible absorption of the circumstellar HI emission by foreground galactic gas and self-absorption, and thus may slightly underestimate the HI mass.

2.2.1. AGB Sources

Stars on the AGB present a large variety of properties in terms of effective temperature, luminosity, chemistry, variability, etc., probably reflecting sources of different ages, initial masses, etc. The observed mass loss rate ranges from 10^{-8} to 10^{-4} M_{\odot} yr $^{-1}$. In fact AGB stars seem to undergo mass loss at a rate which may vary on timescales ranging from a few years to perhaps 10^6 years. We have tried to select oxygen-rich and carbon-rich sources with different variability types and different mass loss rate estimates. Our sample covers also a wide range of stellar temperatures.

Table 1. Observed sources in right ascension order and basic data.

Source	IRAS name	Spectral type	Variability type	Period (days)	d (pc)	T_{eff} (K)	V_{lsr} (km s^{-1})	V_{exp} (km s^{-1})	\dot{M} ($M_{\odot} \text{ yr}^{-1}$)
WX Psc	01037+1219	M8-M10:	Mira	660	650	< 2500	+9	23	$2 \cdot 10^{-5}$
<i>o</i> Cet	02168–0312	M7IIIe+Bep	Mira	332	128	~ 2700	+46	7	$2.5 \cdot 10^{-7}$
ρ Per	03019+3838	M4II	SRb	40	100	3576	+25	≤ 8.5	$1 \cdot 10^{-8}$
NML Tau	03507+1115	M6e-M10e	Mira	462	245	2000-3000	+35	19	$3 \cdot 10^{-6}$
S CMi	07299+0825	M6e-M8e	Mira	332	365	2500-3100	+52	3	$2 \cdot 10^{-7}$
U CMi	07386+0829	M4e	Mira	414	191	3400	+42
RV Hya	08372–0924	M5II	SRc	116	318	3420	–43	5	$3 \cdot 10^{-7}$
U Hya	10350–1307	C5II	SRb	450	162	2965	–31	7	$9 \cdot 10^{-8}$
Y UMa	12380+5607	M7II-III	SRb	168	313	3100	+19	5	$2 \cdot 10^{-7}$
RY Dra	12544+6615	C4,5J	SRb	200	488	2810	–4	13	$1.5 \cdot 10^{-7}$
RT Vir	13001+0527	M8III	SRb	155	138	3034	+17	9	$1 \cdot 10^{-7}$
W Hya	13462–2807	M7.5e-M9ep	SRa	361	115	2500	+41	8	$2 \cdot 10^{-7}$
α^1 Her	17123+1426	M5Ib-II	SRc	...	117	3285	–17	10	$1 \cdot 10^{-7}$
NGC 6369	17262–2343	PN	1550	> 10000	–90	41	...
δ^2 Lyr	18527+3650	M4II	?	60-120	275	3460	–7	≤ 10	$5 \cdot 10^{-8}$
Z Cyg	20000+4954	M5e-M9e	Mira	264	490	< 3300	–148	4	$4 \cdot 10^{-8}$
NGC 7293	22267–2102	PN	200	> 10000	–23	32	...
R Peg	23041+1016	M6e-M9e	Mira	378	350	2300-2900	+24	9	$5 \cdot 10^{-7}$
AFGL 3068	23166+1655	C	Mira	696	1140	1800-2000	–31	14	$1 \cdot 10^{-4}$
AFGL 3099	23257+1038	C	Mira	484	1500	1800-2000	+47	10	$8 \cdot 10^{-6}$
TX Psc	23438+0312	C5II	Lb	...	233	3115	+13	10	$2 \cdot 10^{-7}$
R Cas	23558+5106	M7IIIe	Mira	430	107	< 3000	+25	12	$5 \cdot 10^{-7}$

Oxygen-rich AGB Sources

We discuss first δ^2 Lyr, whose variability type is not defined, and then the 6 oxygen-rich Semi-Regular variables of our sample.

δ^2 **Lyr** (HR 7139) is a relatively warm AGB star (M4II), which is barely variable ($\Delta V \sim 0.2$ mag., Bakos & Tremko 1991). We adopt the effective temperature determined by Sudol et al. (2002) from near-infrared (J and H) interferometry, 3460 ± 160 K. From the profiles of photospheric lines affected by circumstellar absorption, Sanner (1976) finds evidence of an outflow. This source has not been detected in any radio line, but it has an IRAS extended counterpart (Young et al. 1993a). On the other hand, the ISO (3-40 μm) spectrum (Heras et al. 2002) shows no evidence of dust. In Table 1, we adopt the parameters of its wind from Sanner (1976).

The HI spectra are presented in Fig. 1. In this figure, and in the following ones, the horizontal bar represents the velocity extent ($V_{\text{lsr}} \pm V_{\text{exp}}$) expected from the wind parameters given in Table 1 (full line in the case of a CO radio-line determination, dotted line in the case of an optical determination). The contamination is serious especially at $V > -5 \text{ km s}^{-1}$. However, each spectrum clearly shows an HI emission that is increasing with offset up to $\pm 16'$. This indicates that the source has a diameter of $\sim 24'$. The central velocity of the profile and the FWHM agree with those obtained by Sanner (1976). The intensity has been integrated over the 7 NRT beams that contribute to the signal. At a distance of 275 pc, it translates to $\sim 0.075 M_{\odot}$ in atomic hydrogen. As the source has a size of $\sim 24'$ in the East-West direction and as the NRT beam is 22' in the North-South direction, we may have missed part of the HI emission (see Sect. 3.2 for a corrected HI mass).

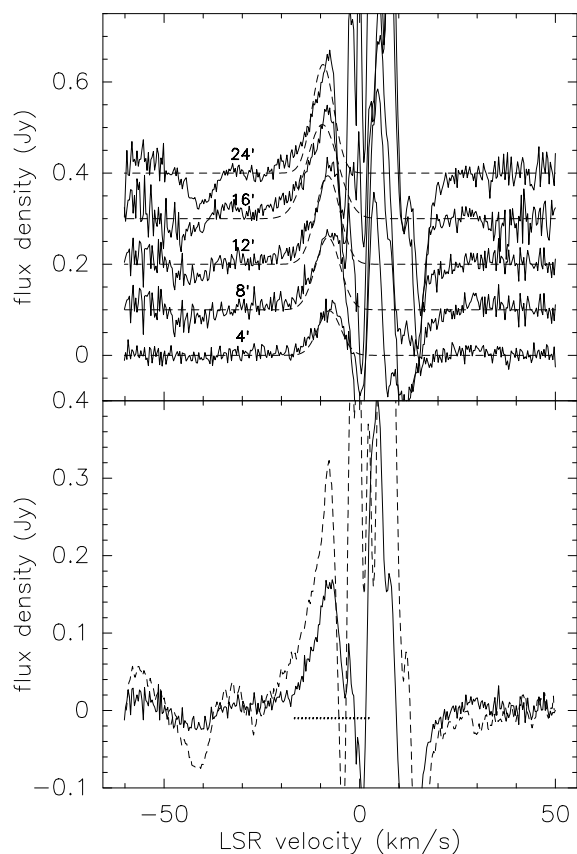


Fig. 1.— Top panel: δ^2 Lyr spectra obtained in the position-switch mode. The off-positions, in this figure and ensuing ones, are indicated in bold characters above each spectrum. For clarity, the individual spectra have been displayed with vertical offsets of 0.05 or 0.1 Jy. Bottom panel: average of these 5 spectra and space integrated intensity scaled by a factor 1/2. The horizontal dashed bar indicates the velocity range expected for circumstellar matter (Sanner 1976).

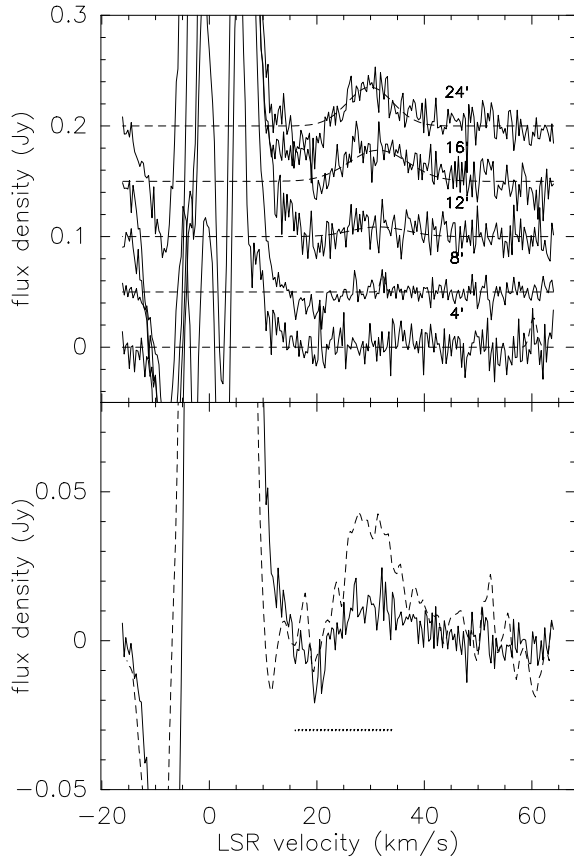


Fig. 2.— Top panel: ρ Per spectra obtained in the position-switch mode. Bottom panel: average of the 5 spectra and space integrated intensity scaled by a factor 1/5. The horizontal dashed bar indicates the velocity range expected for circumstellar matter (Sanner 1976).

ρ **Per** (HR 921) has not been detected in CO, nor in any other radio line. Sanner (1976) finds evidence of an outflow with parameters (V_{lsr} , V_{exp} , \dot{M}) given in Table 1. Mauron & Guilain (1995) detected circumstellar NaI at $5''$ from the central star (i.e. ~ 500 AU), confirming that the star is losing matter. However, the infrared spectrum obtained by ISO shows no evidence of dust around ρ Per (Heras et al. 2002). We adopt the effective temperature from Dumm & Schild (1998).

An HI emission is barely detected in the spectrum obtained with off-positions at $\pm 4'$, whereas it is clearly detected at $\pm 16'$, and at $\pm 24'$ with basically the same intensity (Fig. 2). This indicates that the HI emission is resolved and has a size corresponding to about 7 NRT beams in the East-West direction, i.e. $\sim 24'$. Galactic confusion clearly affects the HI profile near 20 km s^{-1} at ± 16 and $24'$. The blue wing of the HI profile is cut down, which probably results in a displacement of the HI velocity centroid.

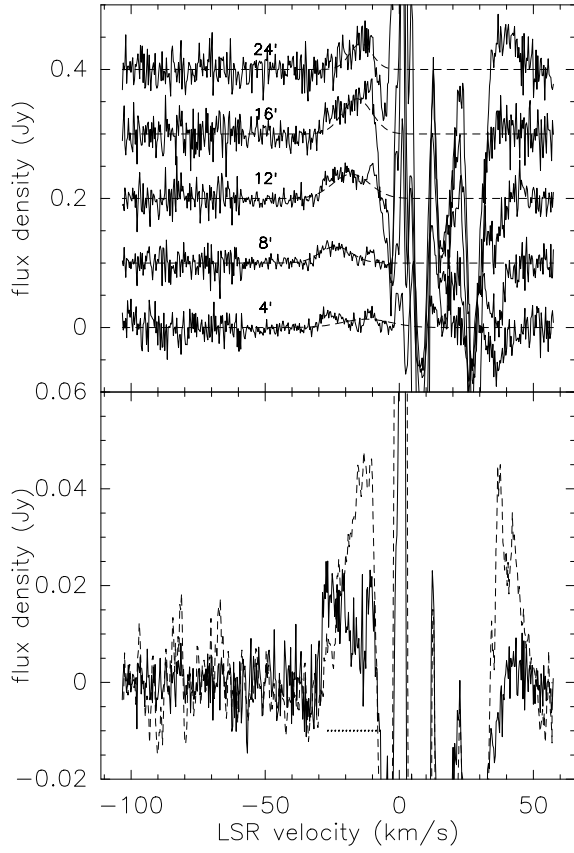


Fig. 3.— Top panel: α^1 Her spectra obtained in the position-switch mode. Bottom panel: average of these 5 spectra and space integrated intensity scaled by a factor 1/5. The horizontal dashed bar indicates the velocity range expected for circumstellar matter (Deutsch 1956).

α^1 **Her** (HR 6406) is known to undergo mass loss since Deutsch (1956) showed that circumstellar lines are present in absorption in the spectrum of its companion, at an angular distance of $5''$. We adopt his wind parameters. Like ρ Per, it was not detected in any radio line (e.g. Heske 1990). Circumstellar K I and Na I were also detected in emission by Mauron & Caux (1992). We adopt the effective temperature determined by Perrin et al. (2004a) from $2 \mu\text{m}$ interferometric data ($T_{\text{eff}} = 3285 \pm 89 \text{ K}$).

The H I emission is increasing with offset (Fig. 3), which indicates that the source has a diameter of the order of $16'$. The central velocity of the profile and its width agree with the parameters obtained by Deutsch (1956). The interstellar confusion is high for $V > -5 \text{ km s}^{-1}$, and seems even to affect the red wing of the profile obtained at $\pm 16'$. An emission component stands out at -10 km s^{-1} . As it can be seen on the individual position-switch spectra at $\pm 4'$, $\pm 8'$, and $\pm 12'$ it is probably real.

RV Hya has been detected in CO by Winters et al. (2003). We adopt their parameters for the wind characteristics. With the temperature scale of normal giants (Ridgway et al. 1980) and an M5 spectral type, the effective temperature should be around 3400 K .

The H I line is marginally detected on the average (Fig. 4). It does not seem to be angularly resolved.

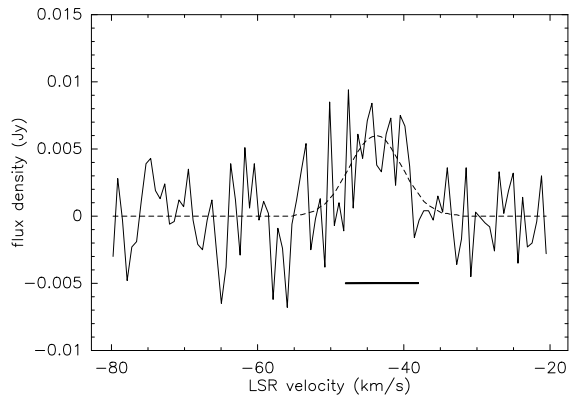


Fig. 4.— Average spectrum of RV Hya obtained in the position-switch mode. The spectral resolution is 0.64 km s^{-1} .

Y UMa is associated to an IRAS extended source (Young et al. 1993a). It has been observed in CO (2–1) by Knapp et al. (1998) and their wind characteristics are given in Table 1. These estimates agree with those obtained by Olofsson et al. (2002). From the temperature scale of normal giants of type later than M6 (Perrin et al. 1998), we adopt an effective temperature of about 3 100 K.

The H I emission is spatially extended ($\phi \sim 8'$, Fig. 5). We note that the central velocity of the H I feature is shifted by $\sim 2 \text{ km s}^{-1}$ with respect to the CO emission and is narrower (Knapp et al. 1998). The profile is probably composite with a narrow component overimposed on a broad faint one. A detailed examination of the separate position-switch data shows that the H I emission is asymmetric and slightly shifted West.

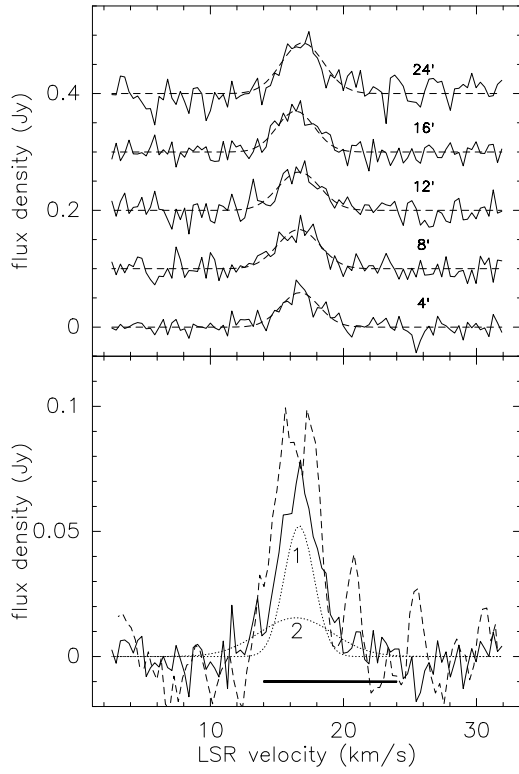


Fig. 5.— Top panel: Y UMa spectra obtained in the position-switch mode. Bottom panel: average of these 5 spectra and space integrated intensity. Gaussian fits to the average are shown to illustrate the decomposition of the profile in 2 components.

RT Vir is also associated to an IRAS extended source (Young et al. 1993a). We adopt the wind characteristics from Knapp et al. (1998). However, Olofsson et al. (2002) derive a larger mass loss rate estimate ($\sim 5 \times 10^{-7} M_{\odot} \text{ yr}^{-1}$, at 170 pc). It has been detected in the thermal ($v=0$, $J=2-1$) SiO line by González Delgado et al. (2003) at a slightly different velocity ($V_{\text{lsr}} \sim 18.6 \text{ km s}^{-1}$). This source was also detected in the OH maser lines at 1 612, 1 665 and 1 667 MHz by Etoke et al. (2003). The effective temperature is taken from Dumm & Schild (1998).

The HI source is extended, $\phi \sim 24'$ (Fig. 6). A detailed examination of the position-switch data shows that the HI emission is asymmetric and shifted East by $\sim 4'$.

W Hya is sometimes classified as a Mira (e.g. Young 1995). It is associated to an IRAS extended source (Young et al. 1993a). We adopt the wind characteristics from Knapp et al. (1998). These parameters agree with those obtained by Young (1995) and Olofsson et al. (2002). The H₂O line at 557 GHz was detected by the Odin satellite and gives consistent parameters for the wind (Justtanont et al. 2005). The circumstellar shell was also detected in K I fluorescence by Guilain & Mauron (1996). Like RT Vir, it has been detected in the OH maser lines at 1612, 1665 and 1667 MHz (Etoka et al. 2003). An effective temperature of $2\,500 \pm 190$ K was obtained by Haniff et al. (1995) from optical interferometry. The stellar disk was also resolved in the radio continuum by Reid & Menten (1997) who derived a (radio) brightness temperature of $1\,500 \pm 570$ K.

The H I source is clearly resolved with a maximum flux reached only at $\pm 16'$ so that we estimate its size to $\sim 24'$ (Fig. 7). The spectra obtained at $\pm 16'$ and $\pm 24'$ show a narrow dip at $+20$ km s⁻¹ (FWHM ~ 3 km s⁻¹), revealing the presence of a small interstellar cloud at $\sim 20'$ East of W Hya.

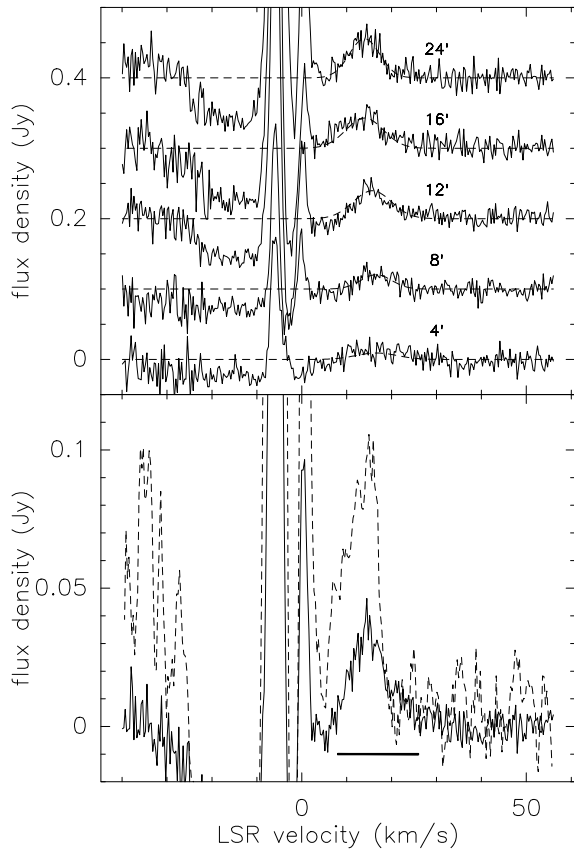


Fig. 6.— Top panel: RT Vir spectra obtained in the position-switch mode. Bottom panel: average of these 5 spectra and space integrated intensity scaled by a factor $1/2$.

We now discuss the 8 oxygen-rich Miras of our sample, in order of increasing spectral type, which corresponds approximately to increasing period and increasing observed mass loss rate. The spectral types of Miras are known to vary with phase, and accordingly the stellar effective temperatures, which makes them particularly uncertain.

U CMi is probably one of the bluest Miras. As it has not been detected in any radio lines, we adopt the radial velocity determined optically (General Catalogue of Stellar Radial Velocities, GCRV). Adopting the effective temperature scale for Mira variables of Dyck et al. (1974), T_{eff} should be around 3400 K.

As there is no estimate available for the expansion velocity, the stellar radial velocity is only marked with a vertical bar (Fig. 8). The H I line is easily detected with a triangular profile centered at a velocity (40.9 km s^{-1}) very close to the stellar one (42 km s^{-1}). It is more intense for $\pm 8'$ than for $\pm 4'$ and we estimate its diameter to $\sim 8'$. As for Y UMa, we observe that the H I emission is not centered on the star position, and slightly shifted West.

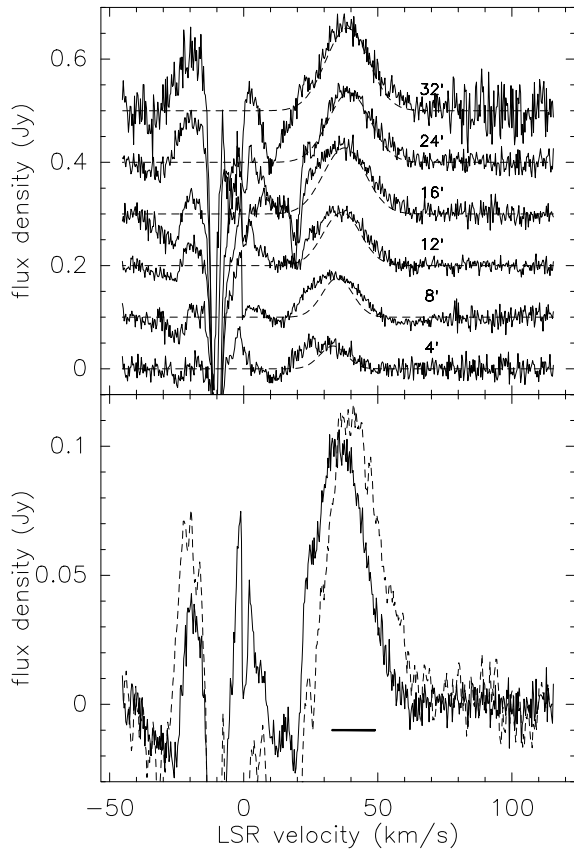


Fig. 7.— Top panel: W Hya spectra obtained in the position-switch mode. Bottom panel: average of these 6 spectra and space integrated intensity scaled by a factor $1/5$.

Z Cyg is remarkable for its high radial velocity suggesting it might belong to population II. It has been detected as an OH maser by Sivagnanam et al. (1989) and in the CO (3-2) line by Young (1995) from whom we adopt the outflow parameters and the distance. The effective temperature should be around 3 300 K or below (Dyck et al. 1974).

An H I line is suspected at $\sim -146 \text{ km s}^{-1}$ (Fig. 9) but we only set an upper limit to its flux.

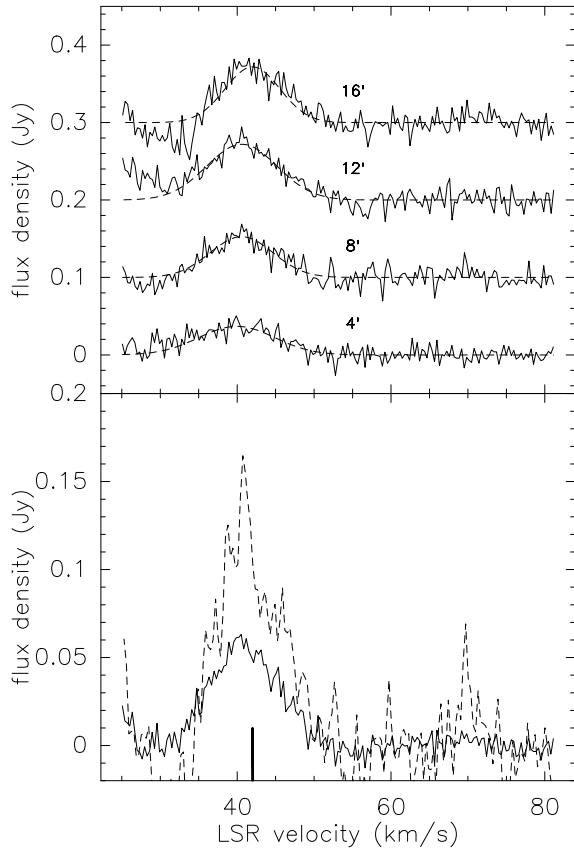


Fig. 8.— Top panel: U CMi spectra obtained in the position-switch mode. Bottom panel: average of these 4 spectra and space integrated intensity.

S CMi has been observed in CO (1–0) and (2–1) by Winters et al. (2003). We adopt their wind parameters and distance based on the period-luminosity relationship for Miras (Feast 1996). The effective temperature should stay most of the time above 2500 K (Dyck et al. 1974).

The H I line is easily detected (Fig. 10) and is slightly more intense for $\pm 8'$ than for $\pm 4'$. As there is no clear difference between $\pm 8'$ and $\pm 12'$ the diameter of the source should be $\sim 8'$.

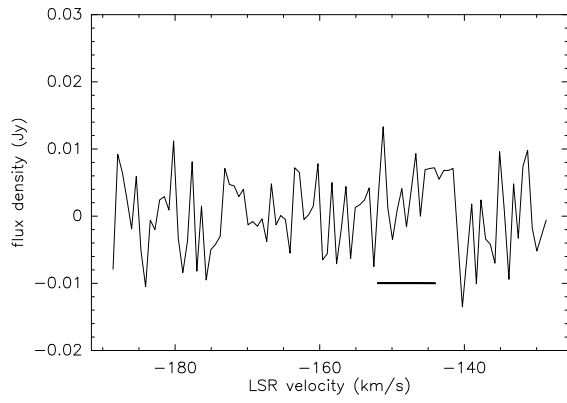


Fig. 9.— Average spectrum of Z Cyg obtained in the position-switch mode. The spectral resolution is 0.64 km s^{-1} .

o **Cet** (Mira, HR 681) has been observed extensively. Its infrared spectrum shows a 10- μ m silicate feature strongly in emission (e.g. Speck et al. 2000). The CO profiles are complex, possibly composite (Knapp et al. 1998; Winters et al. 2003). Circumstellar K I and Na I were also detected by Mauron & Caux (1992). CO (2–1) interferometric and K I data show that the envelope is strongly asymmetric, perhaps bipolar, (Josselin et al. 2000). We adopt a mass loss rate of $2.5 \times 10^{-7} M_{\odot} \text{ yr}^{-1}$ from the detailed modelling of CO rotational lines by Ryde & Schöier (2001). The central star has a hot companion, at approximately $0.5''$ (~ 65 AU), surrounded by a disk accreting a part, $\approx 1\%$, of the matter in the outflow (Reimers & Cassatella 1985).

On the basis of a large set of infrared interferometric data, Weiner (2004) finds that a 2 200 K H₂O shell surrounds a 2 700 K star (at a phase close to maximum). This estimate of the stellar temperature agrees with the Dyck et al. (1974) scale. On the other hand, Perrin et al. (2004b), using near-infrared interferometric data, derive an effective temperature in the range 3 200–3 600 K. These results illustrate that Mira atmospheres have complex structures, as predicted by hydrodynamical models (e.g. Woitke et al. 1999). A prediction of the atomic hydrogen abundance in the stellar atmosphere and inner outflow would certainly require a detailed hydrodynamical and chemical modeling.

o **Cet** was already detected in H I with the VLA (BK1988). These early observations suggest that approximately one third of the hydrogen is atomic when it leaves the star. The source is spatially resolved (radius $\sim 160''$) and slightly offset to the North-West. However this large-scale asymmetry does not seem to be related to the bipolar flow ($\phi \sim 20''$) observed in CO by Josselin et al. (2000).

The signal that we obtained is slightly larger for $\pm 8'$ than for $\pm 4'$ and very stable for larger offsets (Fig. 11). We estimate that the source is just resolved spatially with the NRT ($\phi_{\text{HI}} \sim 8 \pm 4'$), consistent with the result of BK1988 and the extension ($\phi \sim 4.4'$) found by IRAS at 60 μ m (Young et al. 1993a). The average line-profile is of high quality and resembles the triangular shape of the CO line-profiles (e.g. Knapp et al. 1998; Winters et al. 2003), with a small asymmetry shifting the peak (46.3 km s^{-1}) by $\sim 1 \text{ km s}^{-1}$ to the red of the centroid velocity (45.7 km s^{-1}). Such a close agreement, in shape and in position, is exceptional in our sample. But the most important fact maybe that this high-quality H I line-profile clearly does not show the rectangular shape expected from an optically thin envelope with constant expansion velocity (Le Bertre & Gérard, Paper II). This point is further discussed in Sect. 3.

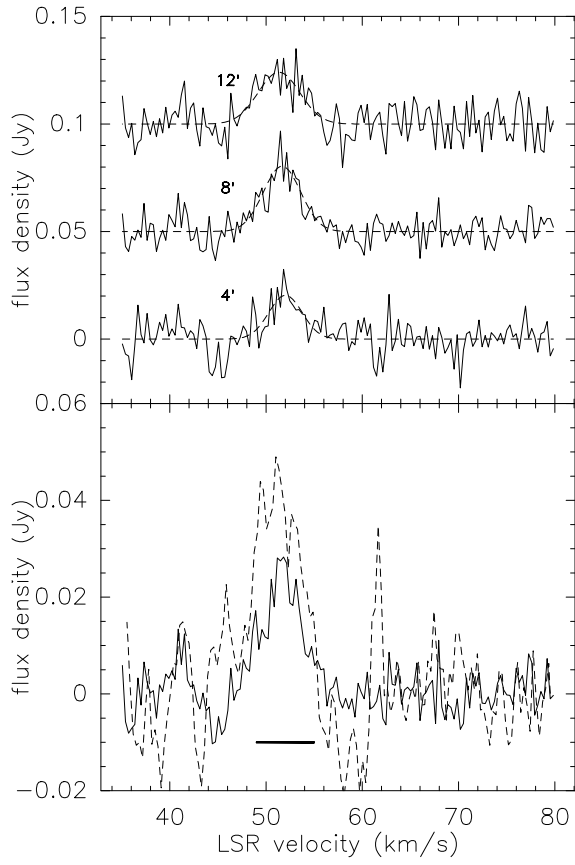


Fig. 10.— Top panel: S CMi spectra obtained in the position-switch mode. Bottom panel: average of these 3 spectra and space integrated intensity.

The integrated intensity is $\sim 0.56 \text{ Jy} \times \text{km s}^{-1}$ which (for a distance of 128 pc) translates into $M_{\text{HI}} \approx 2.2 \times 10^{-3} M_{\odot}$. For comparison, BK1988 find $0.42 \text{ Jy} \times \text{km s}^{-1}$, which is in good agreement with our estimate.

For a size of $8'$ (0.30 pc) and an average expansion velocity of $\sim 4 \text{ km s}^{-1}$, the crossing time is $\sim 38 \times 10^3$ years, and the average mass loss rate in HI over this period is $\sim 0.6 \times 10^{-7} M_{\odot} \text{ yr}^{-1}$. Assuming atomic hydrogen represents 3/4 of the total mass, we find $(\dot{M})_{\text{av}} \sim 0.8 \times 10^{-7} M_{\odot} \text{ yr}^{-1}$ which is one third of the present mass loss rate estimated from CO-lines modelling (Ryde & Schöier 2001). This result is in line with the interpretation of BK1988 that 1/3 of the hydrogen is leaving the star in atomic form.

R Peg has been observed in CO by Young (1995) and Winters et al. (2003). We adopt their wind characteristics. van Belle et al. (1996) obtained interferometric data at $2 \mu\text{m}$ and derived effective temperatures at phases close to maximum ($2333 \pm 100 \text{ K}$), and close to minimum ($2881 \pm 153 \text{ K}$).

As for Y UMa the HI profile seems composite with a narrow component overlaid on a broader one (Fig. 12), and is reminiscent of the Y CVn HI profile (Paper II). Furthermore, the narrow component (1) is spatially resolved with a size of $\sim 16'$. However, the difference in the central velocities of the 2 components is noteworthy. The central velocity of the spectrally broad component (2) seems to agree with the CO one found by Winters et al. (2003), $+24 \text{ km s}^{-1}$, and with those determined from the OH masers: $+23.9 \text{ km s}^{-1}$ for 1667 MHz and $+24.6 \text{ km s}^{-1}$ for 1665 MHz (Sivagnanam et al. 1989).

The examination of the separate position-switch data shows evidence of an offset West with respect to the central star.

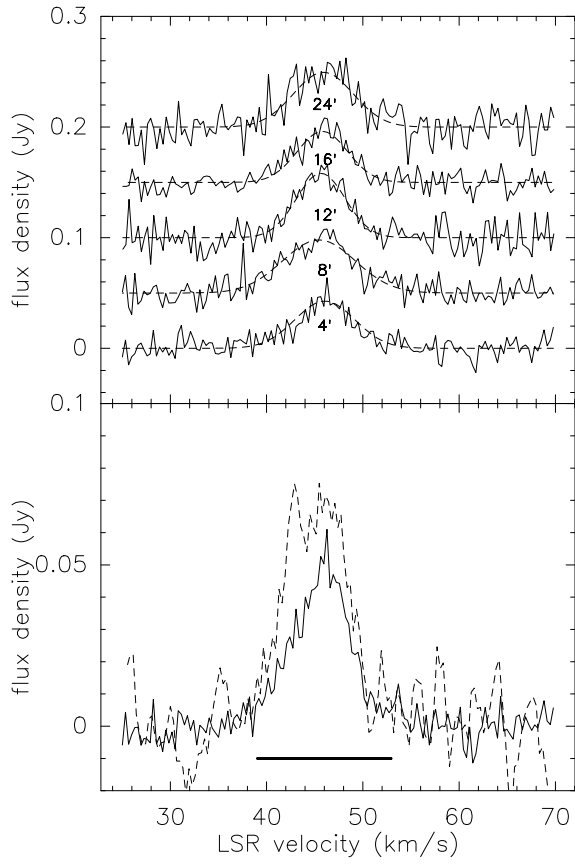


Fig. 11.— Top panel: *o* Cet spectra obtained in the position-switch mode. Bottom panel: average of these 5 spectra and space integrated intensity.

R Cas (HR 9066) has been observed in CO by Young (1995) and Knapp et al. (1998). We adopt their wind characteristics. Neri et al. (1998) have obtained maps in the CO (1–0) and (2–1) lines and find the source to be extended, $\phi \sim 17''$ and $21''$, respectively. It is also associated to a $60 \mu\text{m}$ IRAS extended source of $8.6'$ (Young et al. 1993a). From $2 \mu\text{m}$ interferometric data van Belle et al. (1996) determine an effective temperature of $2954 \pm 174 \text{ K}$, at a phase close to maximum.

The H I source is barely detected at $\pm 4'$ (Fig. 13), but clearly at $\pm 12'$. The diameter is thus $\sim 16'$.

NML Tau (IK Tau) is a large amplitude Mira whose spectral type exhibits important variations with phase (from M6 to M10). It has been detected in CO (1–0) by Knapp & Morris (1985) and Nyman et al. (1992), and mapped in the CO (2–1) line by Neri et al. (1998, $\phi \sim 17''$). This source presents a slightly self-absorbed silicate feature at $10 \mu\text{m}$ (Speck et al. 2000). Adopting the scale for Mira variables of Dyck et al. (1974), the effective temperature should vary in the range 2000–3000 K. We adopt the period from the infrared monitoring of Le Bertre (1993), the distance from the period-luminosity relation for O-rich Miras (Le Bertre & Winters 1998) and the mass loss rate derived from the modelling of the infrared energy distribution (Le Sidaner & Le Bertre 1996). It was not detected in H I by Zuckerman et al. (1980).

Our H I data suffer from interstellar confusion over the velocity range $-40, +40 \text{ km s}^{-1}$. Fig. 14 shows no convincing signal that could be attributed to NML Tau. Over the remaining positive velocity range defined by the CO line-profile ($+40, +54 \text{ km s}^{-1}$) we find an upper limit to the flux density level of 20 mJy , or $0.8 \text{ Jy} \times \text{km s}^{-1}$ over the full CO velocity extent of 38 km s^{-1} . At 245 pc , this limit translates to $M_{\text{HI}} \leq 0.01 M_{\odot}$ in the volume covered by the “on” position of the NRT beam.

This limit applies to an H I emission line. However, some circumstellar matter could be at a low temperature such that atomic hydrogen would appear in absorption against the background (see Sect. 4.3). An upper limit to the background level is given by the sum of the interstellar H I emission around $+35 \text{ km s}^{-1}$ ($\sim 0.5 \text{ K}$) and of the continuum emission at 1420 MHz ($\sim 3.5 \text{ K}$, Reich & Reich 1986), therefore $\sim 4 \text{ K}$.

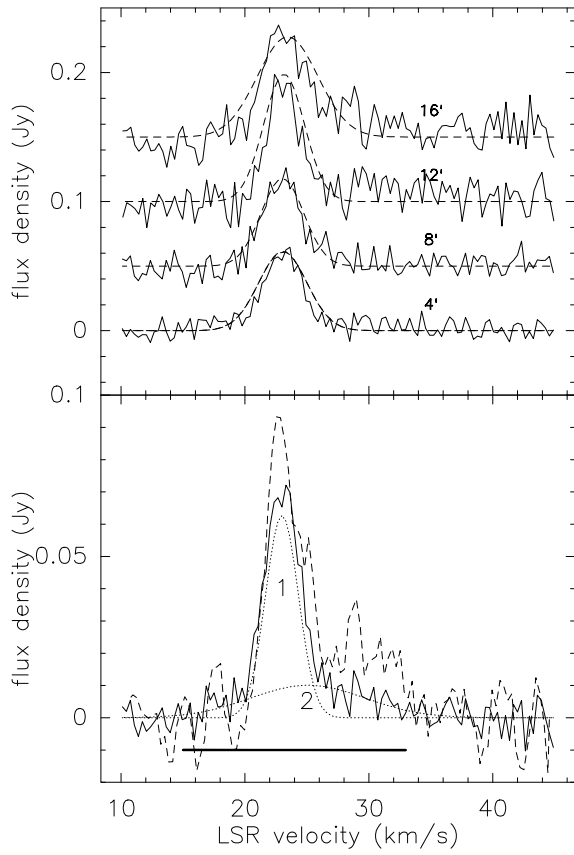


Fig. 12.— Top panel: R Peg spectra obtained in the position-switch mode. Bottom panel: average of these 4 spectra and space integrated intensity scaled by a factor 1/2. Gaussian fits to the average are shown to illustrate the decomposition of the feature in 2 components.

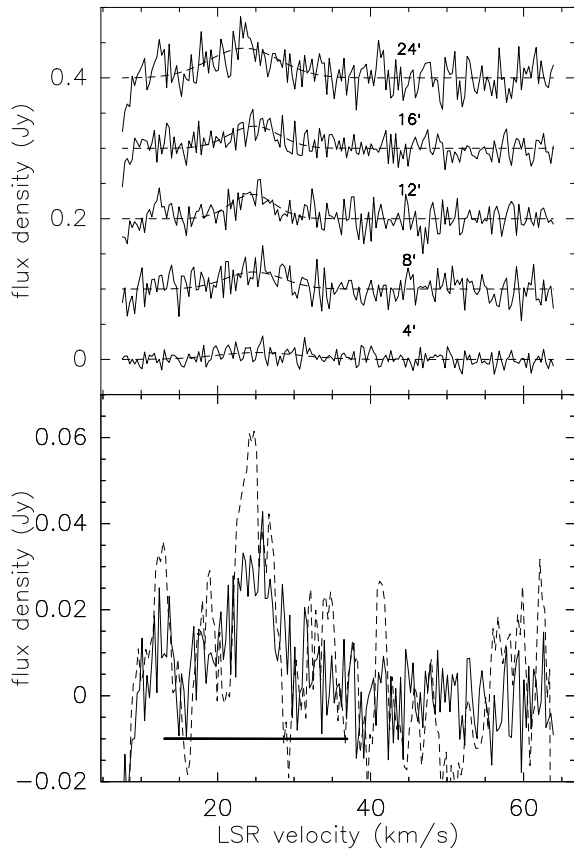


Fig. 13.— Top panel: R Cas spectra obtained in the position-switch mode. Bottom panel: average of these 5 spectra and space integrated intensity scaled by a factor $1/2$.

WX Psc (IRC +10011) is the most extreme oxygen-rich AGB source in our sample and is a representant of the type II OH/IR class, although at a high galactic latitude ($b = -50^\circ$). It has been detected in CO (1–0) by Knapp & Morris (1985). The CO emission has been found to be extended by Neri et al. (1998, $\phi \sim 20''$). The spectral type is probably strongly variable, as for NML Tau. The IRAS Low Resolution Spectrum shows a clear self-absorbed $10\ \mu\text{m}$ silicate feature (Volk & Cohen 1989). The effective temperature should stay most of the time under 2500 K (Dyck et al. 1974). As for NML Tau, we adopt the period from Le Bertre (1993), the distance from Le Bertre & Winters (1998) and the mass loss rate from Le Sidaner & Le Bertre (1996). Zuckerman et al. (1980) also attempted to detect HI at 21 cm, but without success.

Our data suffer from interstellar confusion up to $+10\ \text{km s}^{-1}$ (Fig. 15). As for NML Tau there is no convincing signal that can be attributed to WX Psc. In the region $> 10\ \text{km s}^{-1}$, we can set an upper limit of 5 mJy to the HI emission. Following the same procedure as for NML Tau, we find an upper limit of $0.23\ \text{Jy} \times \text{km s}^{-1}$ to the HI flux within the central beam. At 650 pc, this limit translates to $M_{\text{HI}} \leq 0.02\ M_\odot$ in the volume probed by the “on” position of the NRT beam.

The same caveat as for NML Tau applies if this upper limit is interpreted as an absorption line, the background in that direction being at a level of 4.5 K.

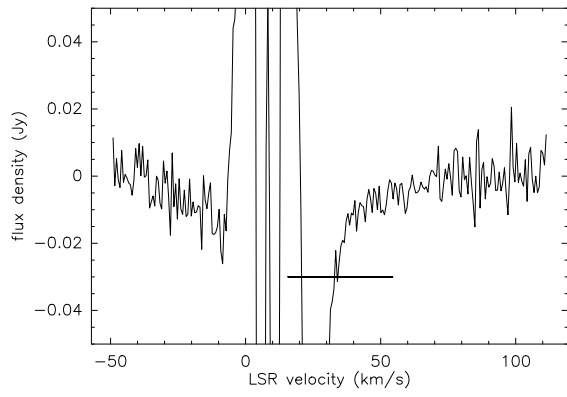


Fig. 14.— Average of all the spectra obtained in the position-switch mode on NML Tau. The spectral resolution is 0.64 km s^{-1} . The horizontal bar indicates the velocity range expected from the CO emission.

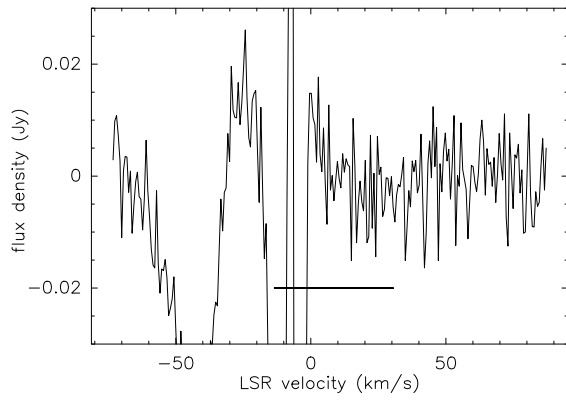


Fig. 15.— Average of all the spectra obtained in the position-switch mode on WX Psc. The spectral resolution is 0.64 km s^{-1} . The horizontal bar indicates the velocity range expected from the CO emission.

Carbon-rich AGB Sources

We first discuss one Irregular and two Semi-Regular variables, then two high mass loss Miras, sometimes referred to as extreme carbon stars (ECS). As in the oxygen-rich cases, the effective temperatures of carbon Miras are variable and very uncertain, particularly since these two are infrared sources.

Table 2. Gaussian fits to the HI profiles, integrated intensities, and atomic hydrogen masses.

Source	confusion	integration time (hours)	Figure	$V_{\text{cent.}}$ (km s ⁻¹)	FWHM (km s ⁻¹)	F_{peak} (mJy)	Flux (Jy × km s ⁻¹)	M_{HI} (M_{\odot})
WX Psc	high/weak	30	15	< 5	< 0.23 ^a	< 0.02 ^a
<i>o</i> Cet	weak	34	11	+45.1	7.7	73	0.56	0.0022
ρ Per	medium	50	2	+30.3	10.6	193	2.05	0.0048
NML Tau	high/weak	31	14	< 20	< 0.76 ^a	< 0.01 ^a
S CMi	weak	27	10	+51.0	5.2	44	0.23	0.0072
U CMi	mean	20	8	+41.3	8.1	119	0.96	0.0083
RV Hya	weak	35	4	-43.8	8.5	6	0.05	0.0012
U Hya	weak	42	17	-30.0	4.9	102	0.50	0.0031
Y UMa	weak	28	5	+16.5	3.7	98	0.36	0.0084
RY Dra	weak	25	18	-4.5	8.5	407	3.46	0.194
RT Vir	mean/weak	24	6	+13.2	9.6	192	1.84	0.0083
W Hya	high/mean	43	7	+41.3	21.8	549	12.0	0.037
α^1 Her	mean/high	46	3	-14.4	11.1	206	2.29	0.0074
NGC 6369	mean	22	21	-91.8	40.5	31	1.26	0.71
δ^2 Lyr	mean/high	21	1	-10.3	5.7	737	4.20	0.075
Z Cyg	weak	27	9	< 6	< 0.05 ^a	< 0.003 ^a
NGC 7293	weak/mean	34	22	-28.7	34.8	530	18.44	0.174
R Peg	weak	30	12	+23.5	5.3	166	0.88	0.025
AFGL 3068	high	23	20	-26.8	30.9	80	2.47	0.76
AFGL 3099	weak	49	19	< 2	< 0.04 ^a	< 0.02 ^a
TX Psc	high	24	16	+9.8	4.2	1250	5.25	0.067
R Cas	mean	33	13	+24.5	5.5	122	0.67	0.0018

^ain the central beam (“on-source”)

TX Psc (HR 9004) has a CO envelope with an irregular structure (Heske et al. 1989). The CO rotational line profiles may be composite with a narrow peak and a broad component (see also Heske 1990). We adopt the wind parameters from Loup et al. (1993) and the effective temperature (3115 ± 130 K) from Bergeat et al. (2001). The source has been found to be extended at $60 \mu\text{m}$ by IRAS (Young et al. 1993a).

The H I signal grows rapidly with increasing offset (Fig. 16). We estimate the H I diameter at $24'$.

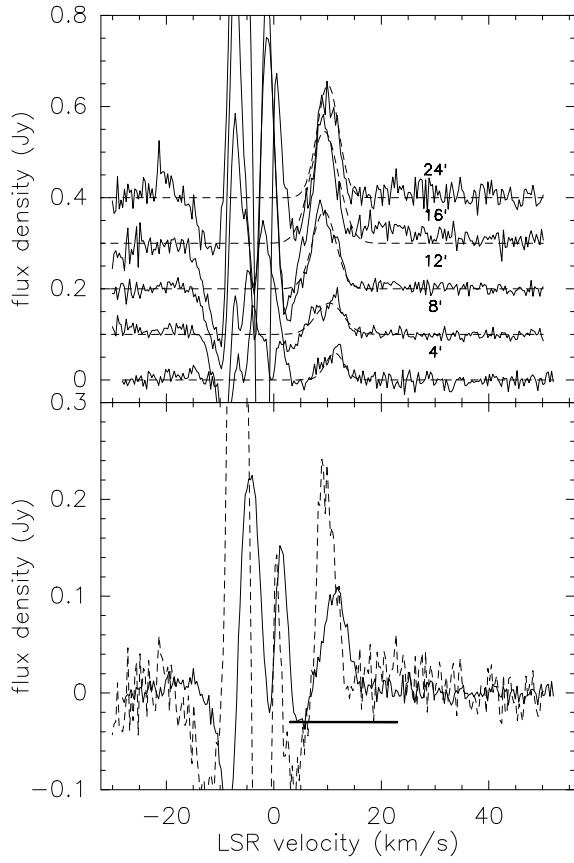


Fig. 16.— Top panel: TX Psc spectra obtained in the position-switch mode. Bottom panel: average of these 5 spectra and space integrated intensity scaled by a factor $1/5$.

U Hya (HR 4163) has been detected in CO (2–1) by Knapp et al. (1998) and we adopt their wind parameters. The IRAS data show a detached dust shell ($\phi \sim 3.5'$) produced by a previous episode of much higher mass loss rate, $\sim 5 \times 10^{-6} M_{\odot} \text{yr}^{-1}$, (Waters et al. 1994). We take the effective temperature from Bergeat et al. (2001).

The H I line is faint (Fig. 17), but well detected on the average spectrum, and might be composite. Also the emission is spatially resolved ($\phi \sim 32'$). Although the flux is weak, this case might be similar to Y CVn.

RY Dra belongs to the rare J-type class, like the star Y CVn which was discussed in Paper II. It has been detected in the ^{12}CO and ^{13}CO rotational lines by Jura et al. (1988), the latter with about half the intensity of the former. The ISO data show a slight evidence of a detached shell that Izumiura & Hashimoto (1999) ascribe to a previous episode of mass loss at a rate of $\sim 10^{-6} M_{\odot} \text{yr}^{-1}$. Furthermore, the IRAS data show a very extended source ($\phi \sim 40'$) at 60 and 100 μm (Young et al. 1993a). We adopt the effective temperature from Bergeat et al. (2001).

The H I source is weakly detected at small offsets (Fig. 18) but reaches more than 50 mJy at $\pm 24'$. The diameter is the largest in our sample, $\sim 40'$.

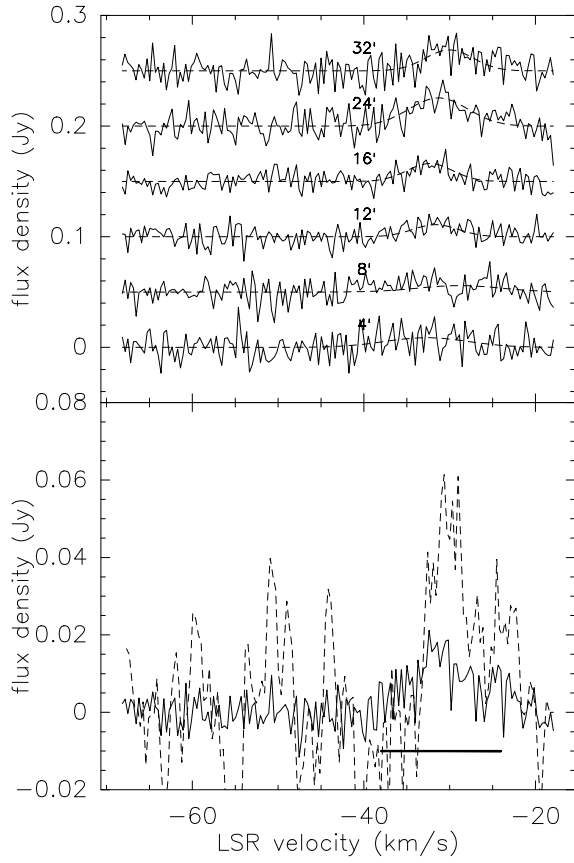


Fig. 17.— Top panel: U Hya spectra obtained in the position-switch mode. Bottom panel: average of these 6 spectra and space integrated intensity scaled by a factor 1/2.

The 2 following sources were discovered in the AFGL infrared survey. Their carbon-rich nature was established from near-infrared spectrophotometry by the presence of the $3.1 \mu\text{m}$ carbon-star absorption feature (Gehrz et al. 1978; Jones et al. 1978).

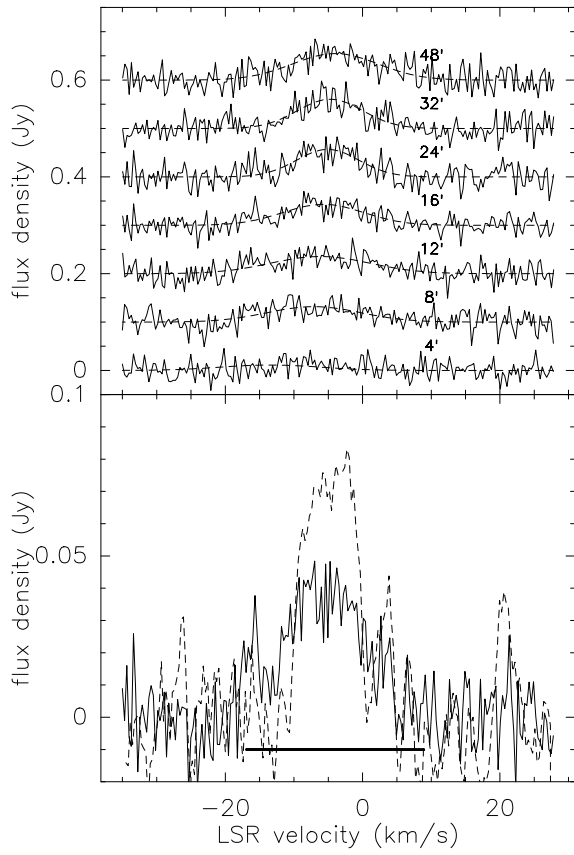


Fig. 18.— Top panel: RY Dra spectra obtained in the position-switch mode. Bottom panel: average of these 7 spectra and space integrated intensity scaled by a factor $1/5$.

AFGL 3099 (IZ Peg) was detected in CO (1–0) by Knapp & Morris (1985). The CO (2–1) emission has been mapped by Neri et al. (1998) and shown to be asymmetric ($14'' \times 7''$). We adopt the period from Le Bertre (1992), the distance from the period-luminosity relationship for carbon Miras (Groenewegen & Whitelock 1996) and the mass loss rate from the modelling of the infrared energy distribution (Le Bertre 1997). There is no stellar spectral classification; however, as the $3.1 \mu\text{m}$ feature is extremely deep (Gehrz et al. 1978), which is an indication of a very low temperature, we adopt the effective temperature for the coolest carbon stars in Bergeat et al. (2001).

We could not detect the source for any beam-throw (up to ± 6 beams, i.e. $\pm 24'$). In Fig. 19 we present the average of all our HI spectra. This is the deepest integration in our survey. In the $30\text{--}80 \text{ km s}^{-1}$ range the HI interstellar background is low and perfectly removed by our procedure, so that we can safely set an upper limit of $2 \times 10^{-3} \text{ Jy}$ to any circumstellar HI emission feature in the central position. Adopting the CO expansion velocity, we find an upper limit of $0.04 \text{ Jy} \times \text{km s}^{-1}$ to the HI emission, which, at a distance of 1.5 kpc, translates to $M_{\text{HI}} \leq 2 \times 10^{-2} M_{\odot}$ in the volume probed by the on-position.

AFGL 3068 (LL Peg) has such a dense wind that the SiC dust feature at $11 \mu\text{m}$ is seen in absorption (Jones et al. 1978). It has been detected in CO (1–0) by Knapp & Morris (1985) and Nyman et al. (1992). The CO (2–1) emission has been mapped by Neri et al. (1998) who suggest the presence of a large ($\phi \sim 17''$) detached bipolar shell. Maunon & Huggins (2006) have detected galactic light scattered by circumstellar dust out to a distance of $\sim 40''$ from the central star with an amazing spiral structure. We adopt the period and the distance from Le Bertre (1992, 1997). A mass loss rate of $5 \times 10^{-5} M_{\odot} \text{ yr}^{-1}$ was derived from a radiative transfer model of the infrared energy distributions by Le Bertre et al. (1995) whereas a consistent time-dependent hydrodynamical model of this source obtained by Winters et al. (1997) gives $\sim 1 \times 10^{-4} M_{\odot} \text{ yr}^{-1}$. As for AFGL 3099, we adopt the effective temperature for the coolest carbon stars (Bergeat et al. 2001).

An emission feature centered at -31 km s^{-1} is barely present at $\pm 4'$, but clearly detected at $\pm 8'$, $\pm 12'$ and $\pm 16'$ (Fig. 20). The intensity is increasing from $\pm 4'$ to $\pm 8'$, but not significantly from $\pm 8'$ to $\pm 16'$. We conclude that HI is detected in emission from AFGL 3068 and that this emission is extended with a size of at least $\sim 8'$ in diameter, or 2.6 pc at 1.14 kpc.

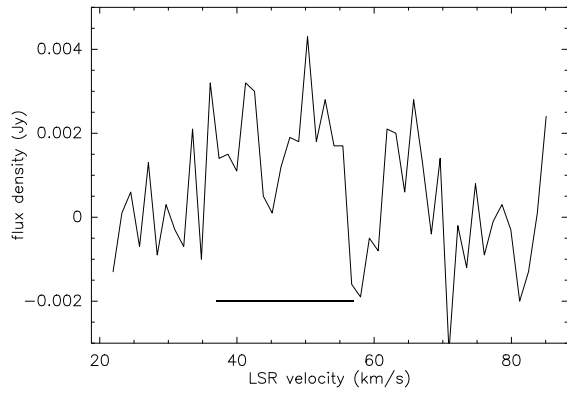


Fig. 19.— Average of all the spectra obtained in the position-switch mode on AFGL 3099. The spectral resolution is 1.28 km s^{-1} . The horizontal bar indicates the velocity range expected from the CO emission.

2.2.2. *PN Sources*

After they have expelled most of their stellar envelope red giants are thought to evolve toward the Planetary Nebula (PN) stage. The mass loss decreases and the hot central core progressively emerges and starts to ionize its surrounding. For some time, a neutral remnant from the AGB circumstellar shell can still be present around an ionized nebula. Recent developments may imply that this scenario applies only to the giants with more massive progenitors, and/or to those that are in a close binary system and experience a common envelope interaction.

“Circumnebular” neutral hydrogen has been detected in absorption against the continuum emitted by the central ionized nebula in 5 PNs by Taylor et al. (1990). Atomic hydrogen has also been detected in emission from IC 418 (Taylor et al. 1989) and from NGC 7293 (R2002).

NGC 6369 (Little Ghost Nebula) is a PN of optical diameter $\sim 40''$. The central star (HD 158269) is an hydrogen-deficient [WC] Wolf-Rayet star. A detailed photoionization model of the nebula by Monteiro et al. (2004) shows that it has a hourglass structure. They derive a nebular mass of $1.8 M_{\odot}$. We adopt the distance derived from this modelling and the expansion velocity ($V_{\text{exp}} = 41.5 \text{ km s}^{-1}$) determined from the [O III] line width by Meatheringham et al. (1988). We note that the [O III] line should probe the ionized central part of the nebula, and that it probably overestimates the expansion velocity of the external medium. Indeed, Garay et al. (1989) have obtained an H76 α linewidth of only 42.8 km s^{-1} . This source has been seen to be extended by IRAS at $25 \mu\text{m}$ ($\phi \sim 1.1'$); this extension could be related to the un-identified 21- μm emission feature reported by Hony et al. (2001).

The source is barely detected at $\pm 4'$ (Fig. 21, but clearly at $\pm 8'$. We estimate its diameter at $8'$.

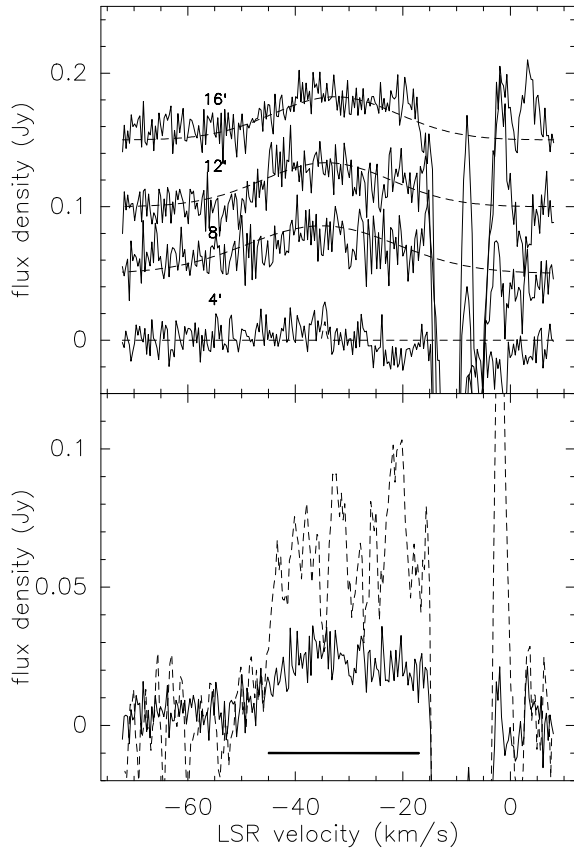


Fig. 20.— Top panel: AFGL 3068 spectra obtained in the position-switch mode. Bottom panel: average of these 4 spectra and space integrated intensity.

NGC 7293 (Helix Nebula) is a nearby PN (~ 200 pc) with a large extent on the sky ($\phi \sim 1000''$). Young et al. (1999) have mapped the nebula in the CO (2–1) line. The CO linewidth is about 63 km s^{-1} . The emission is localized in condensations tracing an expanding equatorial ring that is seen almost pole-on and that surrounds the bright ionized nebula (Huggins et al. 1999). Speck et al. (2002) have obtained H₂ ($v=1-0$) line map which shows that this emission also coincides with the bright nebula. Furthermore they present an H α image which shows a weak and more extended emission, up to $\sim 1100''$ from the central star. This weak emission coincides with dust emission detected by IRAS at 60 and 100 μm , and by ISO at 160 μm . Neutral carbon (C I line at 492 GHz) was detected in several positions on the bright nebula by Young et al. (1997).

NGC 7293 was observed in HI with the VLA (R2002). The emission is fragmented and follows the CO (2–1) ring, except in the South-East quadrant where it is missing. With a diameter of $\sim 16'$, it surrounds the bright optical nebula; in particular it is absent in the central part ($\phi \sim 500''$). R2002 estimate the HI mass to $\sim 0.07 M_{\odot}$. However, from the continuum data at 21 cm, they estimate that they may have missed $\sim 50\%$ (0.67/1.4) of the flux.

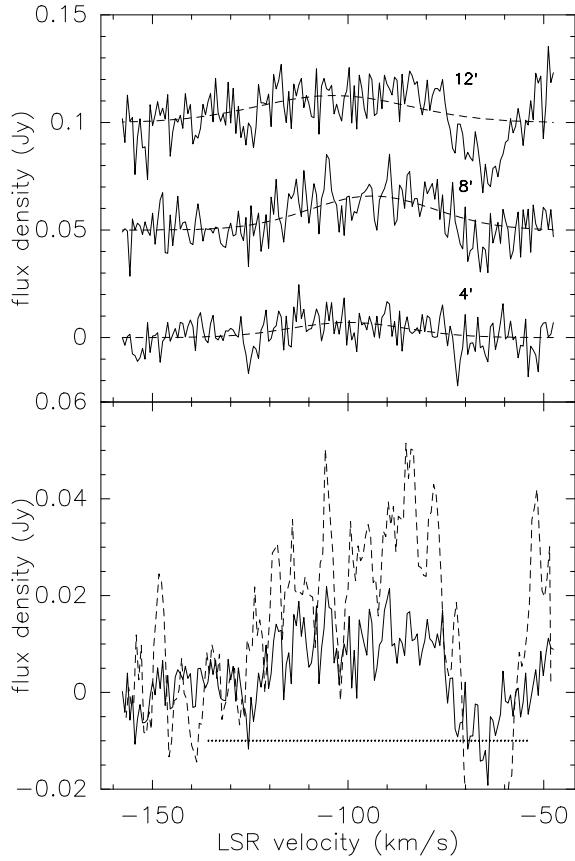


Fig. 21.— Top panel: NGC 6369 spectra obtained in the position-switch mode. The spectral resolution is 0.64 km s^{-1} . Bottom panel: average of these 3 spectra and space integrated intensity. The horizontal dashed bar indicates the velocity range expected from the [O III] line-width (Meatheringham et al. 1998).

The interstellar contamination seems large at $V > -20 \text{ km s}^{-1}$. The source is clearly detected in emission for $V < -20 \text{ km s}^{-1}$ (Fig. 22) and throws larger than $8'$. We detect nearly the same intensity at $\pm 16'$ and $\pm 24'$, and thus evaluate the diameter at $\sim 24'$. This is much larger than estimated by R2002, but consistent with the finding of $\text{H}\alpha$ and dust emissions up to $18'$ from the central star by Speck et al. (2002).

A comparison of our HI spectrum with the spatially integrated spectrum of R2002 shows that the narrow feature at -15 km s^{-1} probably belongs to the source and is not due to confusion, i.e. the contamination may affect our data only at $V > -15 \text{ km s}^{-1}$. Also, the intensity of this feature levels off at $\pm 12'$, an indication that it is not due to the galactic background. Nevertheless we have derived HI line parameters (Table 2) by using only the part of the spectrum outside the range $(-20, +20 \text{ km s}^{-1})$. We find a central velocity $\sim -29 \text{ km s}^{-1}$, instead of -24 km s^{-1} (Young et al. 1999), probably because we excluded the -15 km s^{-1} feature from the fit. Also we observe in our average spectrum a narrow component at -50 km s^{-1} that is not seen in the R2002's spectrum. However, a CO feature is detected at this velocity by Young et al. (1999). The latter is concentrated in the South-East part of the Helix ring where R2002 detect no HI emission.

For the main component centered at -29 km s^{-1} , the examination of the separate position-switch data does not show evidence of a spatial offset with respect to the central star. On the other hand the emission at -15 km s^{-1} is offset to the West. R2002 have mapped this emission with the VLA (their figure 7). The corresponding channel map shows that the feature is located in the North-West and that it could be due to an interaction with the local ISM.

For the main component, we measure an integrated HI intensity of $\sim 18.4 \text{ Jy}\times\text{km s}^{-1}$, which is a factor 2.3 larger than the R2002's estimate. This is in agreement with their finding that, with the VLA, they may have lost $\sim 50\%$ of the flux. The HI emission missed by R2002 is probably diffuse and extends beyond the classical torus of diameter $16'$. The intensity that we missed in the narrow feature at -15 km s^{-1} is only $0.5 \text{ Jy}\times\text{km s}^{-1}$. Considering the extent that we find and the North-South size of our beam ($22'$), it is likely that we also missed HI flux, at the level of $\sim 30 \%$, to the North and to the South of the central source, bringing the total flux to $\sim 28 \text{ Jy}\times\text{km s}^{-1}$. A full map similar to those that we did in Paper II for EP Aqr and Y CVn would be useful.

The HI flux from NGC 7293 is indeed so large that the source can be seen on the Hartmann & Burton (1997) maps obtained at velocities close to -40 km s^{-1} for which the galactic confusion is moderate.

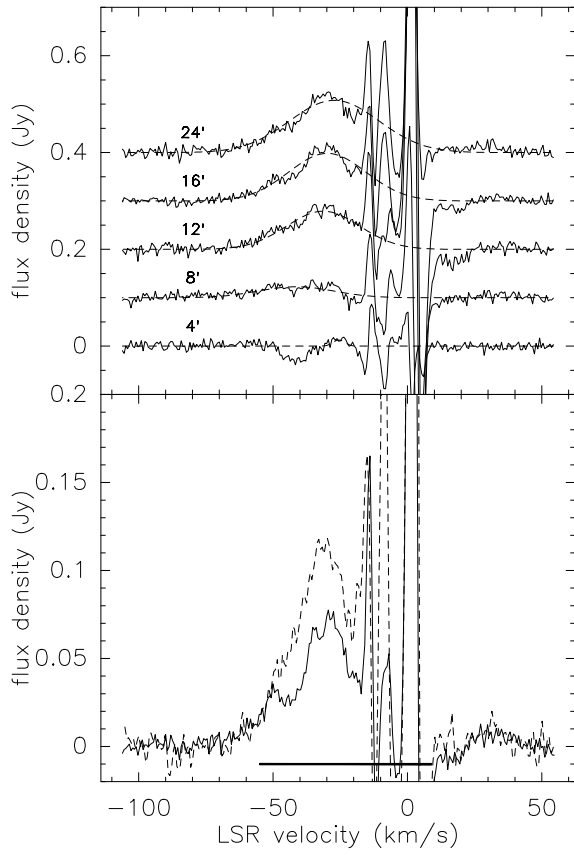


Fig. 22.— Top panel: NGC 7293 spectra obtained in the position-switch mode. The spectral resolution is 0.64 km s^{-1} . Bottom panel: average of these 5 spectra, and space integrated intensity scaled by a factor $1/5$.

3. INTERPRETATION

3.1. Line Profiles

One of the most striking results emerging from our survey is that we find H I line-profiles with a quasi-Gaussian shape, whereas we were expecting rectangular profiles, for unresolved sources, or double-horn ones, for resolved sources. Sometimes the profile seems triangular with a peak close to the centroid velocity (e.g. RT Vir, Fig. 6, or *o* Cet, Fig. 11).

In Paper II, we indeed performed numerical simulations of the H I emission produced by a spherical circumstellar envelope. The emission is assumed to remain optically thin, and its brightness temperature to be proportional to the H I column density. Therefore there is no shell self-absorption and the velocities are radial. In these conditions for an unresolved source with a uniform wind velocity and a constant production rate in atomic hydrogen, the line-profile is rectangular, is centered on the stellar radial velocity, and has a width equal to twice the expansion velocity. For a resolved source, the line profile shows two horns with peaks separated by twice the expansion velocity. These simulations were performed assuming a uniform response within the telescope beam. However, introducing a more realistic response did not significantly change the results (see e.g. figure 7 in Paper III).

We seldom observe double-horn profiles. Only α Her may show such a shape. We also note that NGC 7293 shows several components that could be interpreted as horns. Likewise, the profiles of AFGL 3068 and NGC 6369 could be non-Gaussian. Previously, in a few peculiar cases, we detected a component of the H I emission that might be fitted by a rectangle (RS Cnc, Paper I; EP Aqr, Paper II; X Her, Paper III). In these cases, the width is relatively narrow, $\sim 3\text{-}4 \text{ km s}^{-1}$.

To get centrally peaked profiles we had to assume that the H I velocity is varying with distance from the central star. For resolved sources the velocity has to decrease to zero relative to the stellar radial velocity. A large quantity of hydrogen has to accumulate close to zero velocity, otherwise a deficit appears in the center of the profile. For unresolved sources, the velocity could be assumed to decrease as well as to increase with distance. However, it would be unlikely to get increasing velocities only for unresolved sources, and therefore we can conclude that, on scales probed by the H I emission, the expansion velocity always decreases with distance from the central star. This slowing-down of the circumstellar wind could be due to its interaction with external matter, either remains of previous episodes of mass loss and/or surrounding ISM (Young et al. 1993b; Paper II).

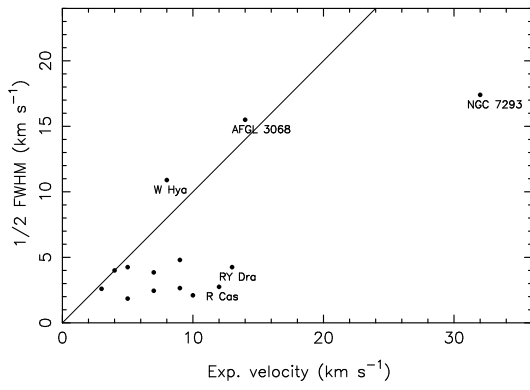


Fig. 23.— Half-FWHM of the HI line versus expansion velocity determined from CO rotational lines.

The slowing-down is also suggested by the comparison of the expansion velocity derived from the CO line-profiles to the half-FWHM of the H I line (Fig. 23). Except for AFGL 3068 and W Hya, the former is always larger than the latter. We note that AFGL 3068 is at a large distance from the galactic plane (~ 740 pc), perhaps in a region devoid of interstellar matter.

In general a gaussian profile can result from thermal and turbulent broadening, as well as from systematic motions of the gas. Presently in our modelling, we are not taking into account thermal and turbulent effects. On the one hand their inclusion in the model may force to reduce the H I outflow velocity because they will provide a supplementary source of line broadening. On the other hand the velocity gradient may have to be reduced and outflow velocities close to 0 (relative to the central star) may not be needed (Libert, Gérard & Le Bertre, in preparation).

3.2. Spatial Distributions

Although the spatial resolution of the NRT is low, most of our sources are so large that they are resolved in the East-West direction. In Table 3 we give estimates of the diameters of the H I sources (col. 3) as explained in Sect. 2.1. For sources that are not resolved with the NRT, we adopt a diameter of $2'$. The four sources that were not detected in H I emission (WX Psc, NML Tau, Z Cyg and AFGL 3099) have not been reported in this Table. We then correct (col. 4) the measured H I mass assuming that the H I emission is circularly symmetric, i.e. it has the same size in declination and in right ascension. The sizes of the H I shells (col. 5) are given for the distances adopted in Table 1. A characteristic timescale (col. 6) can be derived from this size and the FWHM of the H I emission line. Finally from the estimated mass of hydrogen in the circumstellar shell, and assuming that 75 % of the mass is in hydrogen, we derive an average mass loss rate over this timescale (col. 7).

Table 3. Estimated characteristics: sizes, timescales, average mass loss rates.

Source	Chemistry	ϕ_{HI} ($'$)	Total H I mass (M_{\odot})	diameter (pc)	τ (10^3 yr)	$\langle \dot{M} \rangle$ ($M_{\odot} \text{ yr}^{-1}$)	ϕ_{IRAS} ($'$)
<i>o</i> Cet	O	8.	0.0023	0.30	38	0.8×10^{-7}	4.4
ρ Per	O	24.	0.0071	0.70	64	1.5×10^{-7}	...
S CMi	O	8.	0.0076	0.85	160	0.6×10^{-7}	...
U CMi	O	8.	0.0088	0.44	54	2.2×10^{-7}	...
RV Hya	O	2.	0.0012	0.19	21	0.8×10^{-7}	...
U Hya	C	32.	0.0055	1.51	301	0.2×10^{-7}	5.8
Y UMa	O	8.	0.0089	0.73	193	0.6×10^{-7}	7.6
RY Dra	C	40.	0.403	5.68	654	8.2×10^{-7}	37.8 ^a
RT Vir	O	24.	0.0123	0.96	98	1.7×10^{-7}	8.2
W Hya	O	24.	0.055	0.80	36	2.0×10^{-6}	21.0 ^b
α^1 Her	O	16.	0.0091	0.54	48	2.5×10^{-7}	...
NGC 6369	O	8.	0.76	3.6	87	1.2×10^{-5}	...
δ^2 Lyr	O	24.	0.11	1.92	330	4.5×10^{-7}	33.0 ^c
NGC 7293	O	24.	0.258	1.40	39	8.7×10^{-6}	...
R Peg	O	16.	0.031	1.63	301	1.4×10^{-7}	...
AFGL 3068	C	8.	0.81	2.65	84	1.3×10^{-5}	...
TX Psc	C	24.	0.100	1.63	380	3.5×10^{-7}	6.2
R Cas	O	16.	0.0022	0.50	89	0.3×10^{-7}	8.6

^a44.2' at 100 μm

^b30.0' at 100 μm

^c33.8' at 100 μm

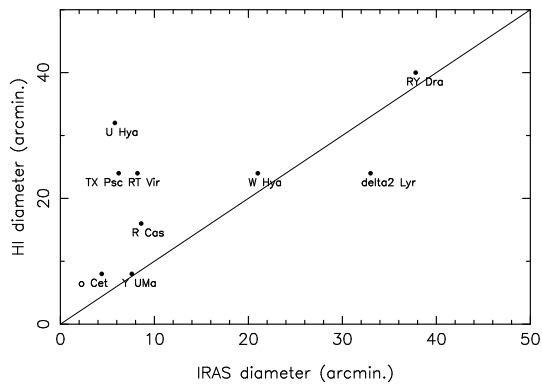


Fig. 24.— HI versus IRAS 60 μm diameter from Young et al. (1993a).

Young et al. (1993a) measured the angular extent of red giants and young PNs in the IRAS 60 and 100 μm survey data. For comparison, we give also the diameter estimated by these authors from the 60 μm IRAS data (col. 8). In general we find sizes in HI that are comparable or larger (Fig. 24). This should not be overemphasized as HI diameters are only rough estimates.

o Cet was barely resolved with the NRT, although it is one of the closest sources in our sample. We find an estimate of the size of the HI source (in the East-West direction) which is consistent with the size of the dust shell estimated from the IRAS data at 60 μm ($R \sim 2.2'$, or 0.08 pc, Young et al. 1993a). We note that BK1988 detected HI emission up to $\sim 160''$ ($2.7'$) from the central star. At the other extreme, AFGL 3068, which is at ~ 1.2 kpc, was angularly resolved with the NRT, $\phi \sim 8'$, or ≥ 2 pc. The HI circumstellar shells of Miras may therefore have very different physical sizes, suggesting very different durations for the past mass loss.

We also note that in the case of AFGL 3068 the HI shell seems much larger than the shell observed in the far-infrared that was not resolved by IRAS (Young et al. 1993a) or by ISO (Izumiura & Hashimoto 1999). This may be an effect of the dust emission dependence on temperature that may impede the detection of matter far from the central star or indicate a relatively recent onset of copious mass-loss rate that is not reflected in the HI spectra. Interestingly, our HI data imply a mass-loss rate about 10 times lower than that given by the detailed modelling of Winters et al. (1997).

ISO observations at 60 and 90 μm of WX Psc show a point source with a FWHM $\sim 1'$ (Hashimoto & Izumiura 2000). For a distance of 650 pc, the circumstellar shell diameter should be at most 0.2 pc. This is interpreted as a recent evolution with a sudden event (< 4000 years) of extremely high mass-loss rate. However, Hashimoto & Izumiura do not exclude the possibility of a faint extended emission that would be the trace of a past mild mass-loss phase. A recent onset of the mass loss in sources like WX Psc or NML Tau (that was not resolved by IRAS, Young 1993a) might explain their non-detection in HI. Indeed in young compact sources with central star effective temperature lower than 2500 K, most of the circumstellar matter may be molecular (see Sect. 4.4).

We have also examined our position-switch data by using separately the two off-positions. The profiles are severely affected by the spatial variations of the background and the resulting spectra suffer much more from galactic HI confusion, which makes them in general difficult to exploit. In some cases (weak/mean confusion, large signal), e.g. RT Vir, U CMi, we can detect the circumstellar emission and observe that it is not symmetric with respect to the central position (i.e. the star position). Nevertheless, this should be taken with caution as the increasing confusion towards 0 km s^{-1} velocity may affect the baselines of the separate

East and West profiles. However, the same effect was noted previously for EP Aqr (Paper II) and X Her (Paper III) for which we also observed shifts in the North-South direction. Finally we note that in the *o* Ceti map obtained with the VLA by BK1988 the H I emission appears offset to the North-West.

From IRAS data at 60 μm Young et al. (1993b) find that among nearby stars Semi-Regular variables are more likely to be resolved than Miras. Our statistics is small but our results (at least for oxygen-rich sources) tend to agree with their conclusion that Semi-Regular variables have been losing mass for a longer duration than Miras. On the other hand they do not find evidence that the shapes of the shells are distorted by interaction with the ISM, which we do (see also Sect. 4.2). Finally, AGB carbon-rich sources appear more extended than oxygen-rich ones. The difference is still more striking when comparing the total H I masses (col. 3 in Table 3). This quantity ranges from 0.001 to 0.1 M_{\odot} for oxygen-rich sources, and from 0.005 to 0.7 M_{\odot} for carbon-rich sources.

The larger extension of carbon-rich sources as compared to oxygen-rich ones is not so surprising as carbon-rich AGB stars should be in a phase of evolution that follows the oxygen-rich stage. And the longer the star loses mass, the larger the mass of its circumstellar shell.

3.3. H I versus CO

We have detected H I emission in sources with and without emission from the CO rotational lines. For instance α^1 Her is detected with a peak intensity ~ 50 mJy at $\pm 12'$, but was not detected in CO by Heske (1990) although the presence of circumstellar matter close to the central star was demonstrated by Deutsch (1956). We note that this situation appears preferentially for warm giants with $T_{\text{eff}} > 3000$ K. It suggests that CO is underabundant in these sources for which the outflows might be mostly atomic. If this suggestion is correct then these sources could be detectable in O I and C I lines, for instance at 492 GHz. Knapp et al. (2000) did not detect C I at 492 GHz from α^1 Her, but this could be an effect of a cyclic variation of the mass loss rate, the region that they probed being only $15''$ in diameter. We also note that our estimate for the average mass loss rate is 2.5 times larger than that of Deutsch (1956).

We sometimes easily detect H I from Semi-Regular variables with low mass loss rates whereas we may not detect it from Miras with large mass loss rates. This may be an effect of the dependence of the $\text{H}_2/\text{H I}$ equilibrium in the stellar atmosphere on temperature. Indeed the stellar effective temperature of the former are larger than 2500 K, and smaller for the

latter, and GH1983 show that hydrogen should be mostly atomic for $T_{\text{eff}} > 2500$ K, and molecular for $T_{\text{eff}} < 2500$ K. Atomic hydrogen should then be present only in the external parts of the circumstellar shells of Miras with large mass loss rates where H_2 is photo-dissociated by the Interstellar Radiation Field. This point is further discussed in Sect. 4.3 and 4.4. CO and HI can trace outflows only where these species are present.

If we now compare CO and HI profiles of sources that show both emissions, we find that, with the notable exception of *o* Cet, they often differ. CO profiles are generally parabolic or rectangular whereas HI profiles are Gaussian or triangular. The HI emission is found within the range encompassed by the CO emission. The HI FWHM is generally smaller than the expansion velocity determined from CO data (Fig. 23). Sometimes its centroid is shifted by $1\text{-}3 \text{ km s}^{-1}$ with respect to the CO centroid. For instance, in Y UMa, we find HI emission from 14 to 20 km s^{-1} with a centroid at 17 km s^{-1} , whereas the CO emission spans from 14 to 24 km s^{-1} and is centered at 19 km s^{-1} (Knapp et al. 1998). Although the kinematics of the outflows should be the same in CO and HI, the regions that are probed by these two tracers are different. Firstly, the beams are different, typically $10\text{-}50''$ for CO observations, and $4' \times 22'$ for our HI observations. Secondly, CO and atomic hydrogen may be present in different zones of the circumstellar shells. For instance CO is expected to be photodissociated by the interstellar radiation field at distances $\sim 10^{16}\text{-}10^{18}$ cm depending on the mass loss rate (Mamon et al. 1990), whereas HI should in general be protected from photo-dissociation by the surrounding ISM. Therefore CO and HI trace different parts of the circumstellar shells. Finally the CO line-profiles and intensities are expected to depend on excitation and optical depth effects much more than for HI.

When we compare the mass loss rates estimated from the H I line profiles to those obtained from CO rotational lines, we do not find any clear trend (Fig. 25). This probably indicates that the mass loss rate varies by an order of magnitude over timescales $\sim 10^5$ years. Nevertheless, we note that Miras tend to lie below the one-to-one line, and Semi-Regulars above it.

It thus appears that the H I line at 21 cm and the CO rotational lines are complementary tracers of the circumstellar outflows and that they are equally needed to describe these media.

4. DISCUSSION

4.1. H I Confusion

In general our data are affected by the large scale structure of the galactic H I emission. Thus the final limits of detection are not set by the sensitivity of the observations but by the effectiveness in removing the galactic emission. When the position-switch procedure has been effective we have qualified the confusion as weak (Table 2). For “medium” and “high” confusion part of the H I spectrum can be affected. It indicates that matter in a direction close to the target and at velocities in the expected range has been detected. In general this matter, that can be at any distance along the line of sight, should not be related to the stellar source.

However, as the central stars may have been undergoing mass loss for a long duration and/or during a previous stage of evolution (e.g. the RGB), in some cases it might be that this matter (or part of it) is physically related to the source. For instance, the interaction of the outflow with its surrounding leads to the formation of a shell made of compressed circumstellar material and swept-up circumstellar/interstellar matter (Sect. 3.1). The matter in this shell should be at velocity close to the central star velocity. If part of the material lost by the central star is mixed in position and in velocity with the surrounding ISM, we may never be able to get an exhaustive balance of the mass lost by the central stars. For instance, in their H I study of IC 418, Taylor et al. (1989) noted that part of the detected hydrogen, blueshifted with respect to the PN system velocity, cannot be identified unambiguously as circumstellar or interstellar matter.

4.2. Interaction with the ISM

For several sources we observe a shift between the central velocities of the H I and CO lines ($\sim 1\text{-}3 \text{ km s}^{-1}$). In some cases we also observe an offset of the H I source with respect to the stellar position ($\sim 1\text{-}4'$). Such a kind of offset has not been observed in CO. Since the H I emission profiles show evidence of a slowing-down of the stellar outflows by the surrounding ISM (Paper II and III, Sect. 3.1), and since the central stars are moving with respect to the ISM², we may suspect that these velocity shifts and spatial offsets are due to a non-isotropic interaction between the outflows and the ISM. One may also consider a gradient in the ISM density that would induce a non-isotropic slowing-down of the circumstellar outflow.

In order to corroborate this hypothesis we have used the non-spherical model of H I emission developed by Gardan et al. (2006, Paper III). As an example we consider a source located at 140 pc with an outflow corresponding to a mass loss in atomic hydrogen of $5 \times 10^{-7} M_{\odot} \text{ yr}^{-1}$, and that is initially spherical and isotropic. The velocity is taken to decrease linearly from an inner boundary located at $0.1'$ (or $4 \times 10^{-3} \text{ pc}$) from the central star. To simulate a non-isotropic interaction, we adopt a velocity law as :

$$V = 10.0 - (1.43 + 0.41 \cos \alpha) \times (r - 0.1) \quad (4)$$

with V expressed in km s^{-1} , r in $'$, and α being a polar angle. The slowing down of the outflow is maximum for $\alpha = 0^{\circ}$ and minimum for $\alpha = 180^{\circ}$. The geometry of the circumstellar shell is thus progressively becoming egg-shaped. For this test, we adopt a typical duration of 50×10^3 years, such that the outer boundary is located at $5'$ (0.2 pc) for $\alpha = 0^{\circ}$, with $V = 1 \text{ km s}^{-1}$, and $7.2'$ ($\sim 0.3 \text{ pc}$) for $\alpha = 180^{\circ}$, with $V \sim 2.8 \text{ km s}^{-1}$. We adopted for the NRT beam a “sinc” response (see Paper III).

The results of such a simulation are given in Fig. 26. The polar axis of the source ($\alpha = 0^{\circ}$) is first placed in the plane of the sky pointing East (Fig. 26, left). The H I profiles are symmetric and centered on the stellar velocity, but the emission feature is more pronounced East than West. If the polar axis is pointing 90° away from the observer (Fig. 26, right), the H I profile becomes asymmetric with a red-shifted peak. In that case the emission remains centered on the star position. Finally, if the polar axis is oriented 45° away from the observer and at a position angle of 90° (Fig. 26, center), the H I profile is asymmetric and the emission is stronger East of the central star.

²although this cannot be strictly demonstrated, we note that our sources are close to the Sun and have a non-zero V_{lsr}

This simulation shows that a slowing-down of the stellar outflow more pronounced in a given direction could produce either a shift in velocity of the H I emission line, or an offset in position of this emission, or a combination of both. This effect may add to an intrinsic asymmetry due to the mass loss from the central star, as we showed for X Her (Paper III).

4.3. Cold Atomic Hydrogen

We have detected H I in emission towards AFGL 3068. However, we have previously reported the detection of H I *in absorption* towards a similar source, IRC +10216, (Le Bertre & Gérard 2001), indicating that the gas in the outflow cools down to a temperature below 4 K. Such a low temperature was predicted for high mass loss rate AGB stars as a result of adiabatic expansion (Jura et al. 1988; Sahai 1990). At first sight it is puzzling that we do not observe the same effect in AFGL 3068 of mass loss rate about 5 times larger. However the distances to these sources differ by a factor ~ 8 , so that the NRT beam scales as $0.16 \text{ pc} \times 0.86 \text{ pc}$ for IRC +10216 as compared to $1.3 \text{ pc} \times 7.3 \text{ pc}$ for AFGL 3068. Therefore, in the case of AFGL 3068 we have explored a very external region where grain photo-electric heating might become important. For instance, in their models of IRC +10216, Crosas & Menten (1997) and Groenewegen et al. (1998) predict that the temperature should increase at $r \geq 0.1 \text{ pc}$ due to this effect (although their minima are still higher than our observational upper limit).

The H I detection of IRC +10216 in absorption and of AFGL 3068 in emission might then be explained as a combined effect of beam size and distance. If this is correct, the H I mass that we have derived for AFGL 3068 may be underestimated due to absorption against the background.

The gas temperature in the circumstellar envelopes depends strongly on the mass-loss rate (e.g. Jura et al. 1988). It is expected to be larger in the sources with low mass-loss rate ($\sim 10^{-7} M_{\odot} \text{ yr}^{-1}$) than in those with high mass-loss rate ($\sim 10^{-5} M_{\odot} \text{ yr}^{-1}$). Low mass-loss rate sources, and in particular Semi-Regular Variables, are therefore less liable to contain very cold atomic hydrogen in their envelopes. On the other hand, this effect may concern Miras with substantial mass loss rate, like WX Psc or NML Tau.

4.4. Molecular Hydrogen

Hydrogen in stars with low atmospheric temperature ($T_{\star} \leq 2500 \text{ K}$) should be molecular (GH1983). The expected lifetime of molecular hydrogen in the ISM is ~ 1000 years for a

standard Interstellar Radiation Field (Le Petit et al. 2002). This translates to $r \sim 10^{-3}$ or 10^{-2} pc for an average expansion velocity of 1 or 10 km s^{-1} , respectively. However, molecular hydrogen is self-shielded (Morris & Jura 1983) and the real extent of an H_2 circumstellar envelope depends on the mass loss rate and the velocity field. For instance GH1983 estimate that, for a mass loss rate of $4 \times 10^{-5} \text{ M}_\odot \text{ yr}^{-1}$ and a uniform expansion velocity of 16 km s^{-1} , the radius of the molecular envelope would be ~ 0.2 pc.

It is therefore important to check the presence of atomic hydrogen at large distance from the central star for those with low effective temperature. As sources with low effective temperature are also those with presently high mass-loss rate (e.g. WX Psc, NML Tau), atomic hydrogen may be detected in these sources, either in absorption or in emission, only at large distances from the central stars, and, of course, only if mass loss has been operating for a long enough time.

5. CONCLUSION

We have undertaken a search for the HI line at 21 cm in the direction of AGB stars and related sources. We have detected circumstellar HI in a variety of sources sampling the post main-sequence evolution of low and intermediate mass stars. The emissions are extended indicating shell sizes from 0.2 pc to more than 2 pc. The HI line can therefore be used to trace the mass loss history for long periods, up to several 10^5 years. However, we may have missed atomic hydrogen at low temperature ($< 10 \text{ K}$) and hydrogen locked into H_2 .

For some sources (ρ Per, α Her, δ^2 Lyr, U CMi) our HI detection is the first radio detection.

The HI line-profiles indicate that the outflows are slowing down, probably due to the interaction with surrounding matter. Furthermore, we observe offsets in velocity and spatial asymmetries that indicate a distortion of the outflows. These effects were already noted for EP Aqr (Paper II) and for X Her (Paper III), and seem frequent. They could be connected to the motion of the sources with respect to the local ISM, or to its inhomogeneity, as well as to the mass ejection process itself.

We are grateful to the referee for his/her detailed review that helped us improve our paper. The Nançay Radio Observatory is the Unité scientifique de Nançay of the Observatoire de Paris, associated as Unité de Service et de Recherche (USR) No. B704 to the French Centre National de la Recherche Scientifique (CNRS). The Nançay Observatory also gratefully acknowledges the financial support of the Conseil Régional de la Région Centre in

France. This research has made use of the SIMBAD database, operated at CDS, Strasbourg, France and of the NASA's Astrophysics Data System.

Facilities: NRT

REFERENCES

- Bakos, G.A., & Tremko, J. 1991, *Contr. Astron. Obs. Skalnaté Pleso*, 21, 99
- Bergeat, J., Knapik, A., & Rutily, B. 2001, *A&A*, 369, 178
- Bowers, P.F., & Knapp, G.R. 1988, *ApJ*, 332, 299 (BK1988)
- Crosas, M., & Menten, K.M. 1997, *ApJ*, 483, 913
- Deutsch, A.J. 1956, *ApJ*, 123, 210
- Dumm, T., & Schild, H. 1998, *New Astronomy*, 3, 137
- Dyck, H.M., Lockwood, G.W., & Capps, R.W. 1974, *ApJ*, 189, 89
- Etoka, S., Le Squeren, A.M., & Gérard, E. 2003, *A&A*, 403, L51
- Feast, M.W. 1996, *MNRAS*, 278, 11
- Garay, G., Gathier, R., Rodríguez, L.F. 1989, *A&A*, 215, 101
- Gardan, E., Gérard, E., & Le Bertre, T. 2006, *MNRAS*, 365, 245 (Paper III)
- Gehrz, R.D., Hackwell, J.A., & Briotta, D. 1978, *ApJ*, 221, L23
- Gérard, E., & Le Bertre, T. 2003, *A&A*, 397, L17 (Paper I)
- Glassgold, A.E., & Huggins, P.J. 1983, *MNRAS*, 203, 517 (GH1983)
- González Delgado, D., Olofsson, H., Kerschbaum, F., Schöier, F.L., Lindqvist, M., & Groenewegen M.A.T. 2003, *A&A*, 411, 123
- Groenewegen, M.A.T., van der Veen, W.E.C.J., & Matthews, H.E. 1998, *A&A*, 338, 491
- Groenewegen, M.A.T., & Whitelock, P.A. 1996, *MNRAS*, 281, 1347
- Guilain, C., & Mauron, N. 1996, *A&A*, 314, 585
- Haniff, C.A., Scholz, M., & Tuthill, P.G. 1995, *MNRAS*, 276, 640

- Hartmann, D., & Burton, W.B. 1997, Atlas of Galactic Neutral Hydrogen, Cambridge University Press
- Hashimoto, O., & Izumiura, H. 2000, *Advances in Space Research*, 25, 2197
- Heras, A.M., Shipman, R.F., Price, S.D., et al. 2002, *A&A* 394, 539
- Heske, A. 1990, *A&A*, 229, 494
- Heske, A., te Lintel Hekkert, P., & Maloney, P.R. 1989, *A&A*, 218, L5
- Hony, S., Waters, L.B.F.M., & Tielens, A.G.G.M. 2001, *A&A*, 378, L41
- Huggins, P.J., Cox, P., Forveille, T., Bachiller, R., & Young, K. 1999, IAU S191, 425
- Izumiura, H., & Hashimoto, O. 1999, IAU S191, 401
- Jones, B., Merrill, K.M., Puetter, R.C., & Willner, S.P. 1978, *AJ*, 83, 1437
- Josselin, E., Mauron, N., Planesas, P., & Bachiller, R. 2000, *A&A*, 362, 255
- Jura, M., Kahane, C., & Omont, A. 1988, *A&A*, 201, 80
- Justtanont, K., Bergman, P., Larsson, B., et al. 2005, *A&A*, 439, 627
- Knapp, G.R., Crosas, M., Young, K., & Ivezić, Ž. 2000, *ApJ*, 534, 324
- Knapp, G.R., & Morris, M. 1985, *ApJ*, 292, 640
- Knapp, G.R., Young, K., Lee, E., & Jorissen, A. 1998, *ApJS*, 117, 209
- Lamers, H.J.G.L.M., & Cassinelli, J.P. 1999, *Introduction to Stellar Winds*, Cambridge University Press
- Le Bertre, T. 1992, *A&AS*, 94, 377
- Le Bertre, T. 1993, *A&AS*, 97, 729
- Le Bertre, T. 1997, *A&A*, 324, 1059
- Le Bertre, T., & Gérard, E. 2001, *A&A*, 378, L29
- Le Bertre, T., & Gérard, E. 2004, *A&A*, 419, 549 (Paper II)
- Le Bertre, T., Gougeon, S., & Le Sidaner, P. 1995, *A&A*, 299, 791
- Le Bertre, T., & Winters J.M. 1998, *A&A*, 334, 173

- Le Petit, F., Roueff, E., & Le Bourlot, J. 2002, *A&A*, 390, 369
- Le Sidaner, P., & Le Bertre, T. 1996, *A&A*, 314, 896
- Loup, C., Forveille, T., Omont, A., & Paul, J.F. 1993, *A&AS*, 99, 291
- Mamon, G.A., Glassgold, A.E., & Huggins, P.J. 1990, *ApJ*, 328, 797
- Mauron, N., & Caux, E. 1992, *A&A*, 265, 711
- Mauron, N., & Guilain, C. 1995, *A&A*, 298, 869
- Mauron, N., & Huggins, P.J. 2006, *A&A*, 452, 257
- Meatheringham, S.J., Wood, P.R., & Faulkner, D.J. 1988, *ApJ*, 334, 862
- Monteiro, H., Schwarz, H.E., Gruenwald, R., & Heathcote, S. 2004, *ApJ*, 609, 194
- Morris, M., & Jura, M. 1983, *ApJ*, 264, 546
- Neri, R., Kahane, C., Lucas, R., Bujarrabal, V., & Loup, C. 1998, *A&AS*, 130, 1
- Nyman, L.-Å., Booth, R.S., Carlström, U., et al. 1992, *A&AS*, 93, 121
- Olofsson, H., González Delgado, D., Kerschbaum, F., & Schöier, F.L. 2002, *A&A*, 391, 1053
- Perrin, G., Coudé du Foresto, V., Ridgway, S.T., et al. 1998, *A&A*, 331, 619
- Perrin, G., Ridgway, S.T., Coudé du Foresto, V., et al. 2004a, *A&A*, 418, 675
- Perrin, G., Ridgway, S.T., Mennesson, B., et al. 2004b, *A&A*, 426, 279
- Reich, P., & Reich, W. 1986, *A&AS*, 63, 205
- Reid, M.J., & Menten, K.M. 1997, *ApJ*, 476, 327
- Reimers, D., & Cassatella, A. 1985, *ApJ*, 297, 275
- Ridgway, S.T., Joyce, R.R., White, N.M., & Wing, R.F. 1980, *ApJ*, 235, 126
- Rodríguez, L.F., Goss, W.M., & Williams, R. 2002, *ApJ*, 574, 179 (R2002)
- Ryde, N., & Schöier, F.L. 2001, *ApJ*, 547, 384
- Sahai, R. 1990, *ApJ*, 362, 652
- Sanner, F. 1976, *ApJS*, 32, 115

- Sivagnanam, P., Le Squeren, A.M., Foy, F., & Tran Minh, F. 1989, *A&A*, 211, 341
- Speck, A.K., Barlow, M.J., Sylvester, R.J., & Hofmeister, A.M. 2000, *A&AS*, 146, 437
- Speck, A.K., Meixner, M., Fong, D., McCullough, P.R., Moser, D.E., & Ueta, T. 2002, *AJ*, 123, 346
- Sudol, J.J., Benson, J.A., Dyck, H.M., & Scholz, M. 2002, *AJ*, 124, 3370
- Taylor, A.R., Gussie, G.T., & Goss, W.M. 1989, *ApJ*, 340, 932
- Taylor, A.R., Gussie, G.T., & Pottasch, S.R. 1990, *ApJ*, 351, 515
- van Belle, G.T., Dyck, H.M., Benson, J.A., & Lacasse, M.G. 1996, *AJ*, 112, 2147
- van Driel W., Pezzani J., & Gérard E. 1996, in “High Sensitivity Radio Astronomy”, N. Jackson & R.J. Davis (eds.), Cambridge Univ. Press, p. 229
- Volk, K., & Cohen, M. 1989, *AJ*, 98, 931
- Waters, L.B.F.M., Loup, C., Kester, D.J.M., Bontekoe, Tj.R., & de Jong, T. 1994, *A&A*, 281, L1
- Weiner, J. 2004, *ApJ*, 611, L37
- Winters, J.M., Fleischer, A.J., Le Bertre, T., & Sedlmayr, E. 1997, *A&A*, 326, 305
- Winters, J.M., Le Bertre, T., Jeong, K.S., Nyman, L.-Å., & Epchtein, N. 2003, *A&A*, 409, 715
- Woitke, P., Helling, C., Winters, J.M., & Jeong, K.S. 1999, *A&A*, 348, L17
- Young, K. 1995, *ApJ*, 445, 872
- Young, K., Cox, P., Huggins, P.J., Forveille, T., & Bachiller, R. 1997, *ApJ*, 482, L101
- Young, K., Cox, P., Huggins, P.J., Forveille, T., & Bachiller, R. 1999, *ApJ*, 522, 387
- Young, K., Phillips, T.G., & Knapp, G.R. 1993a, *ApJS*, 86, 517
- Young, K., Phillips, T.G., & Knapp, G.R. 1993b, *ApJ*, 409, 725
- Zuckerman, B., Terzian, Y., & Silverglate, P. 1980, *ApJ*, 241, 1014

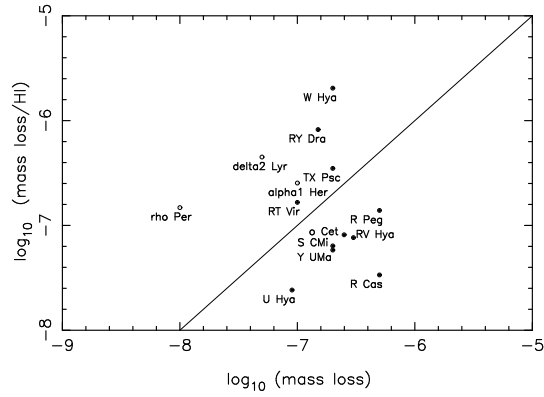


Fig. 25.— Average mass loss rate estimated from HI versus mass loss rate from the literature (Table 1). Filled circles: mass loss rates derived from CO rotational lines; empty circles: mass loss rates derived from optical data (Deutsch 1956; Sanner 1976).

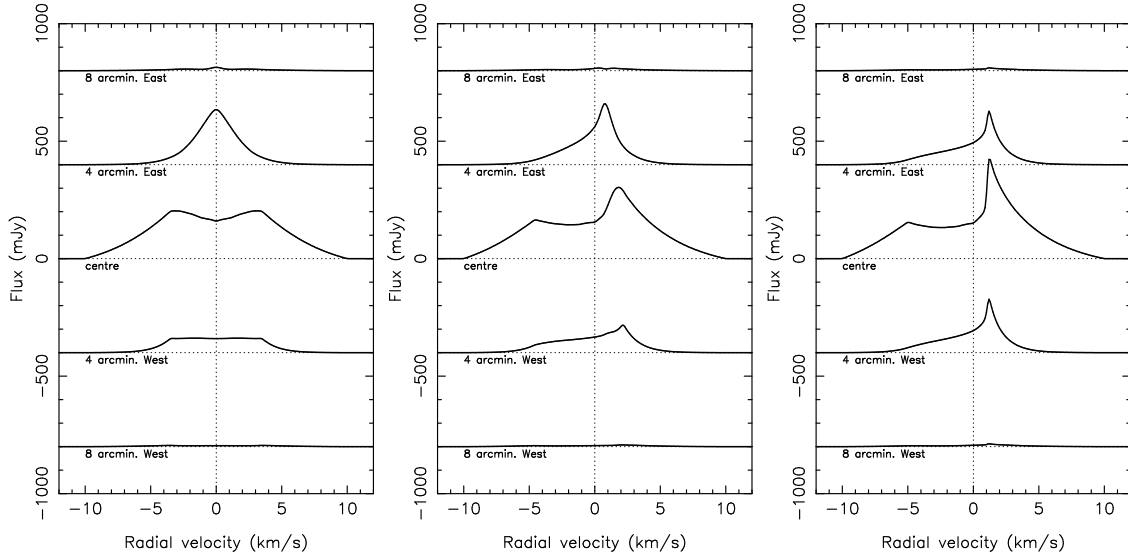


Fig. 26.— Simulation of the HI emission from an egg-shaped circumstellar shell (see Sect. 4.2). Left : PA = 90°, inclination angle = 0°; centre : PA = 90°, inclination angle = -45°; right : PA = 90°, inclination angle = -90°.